MATHEMATICAL MODEL AND EXPERIMENTAL DESIGN OF AN AIR-FILLED ALPHA STIRLING REFRIGERATOR

An Honors Undergraduate Thesis

Submitted to the Department of Aerospace and Mechanical Engineering of the University of Notre Dame

by

Patrick K. McFarlane

_____

Fabio Semperlotti, Advisor

Department of Aerospace and Mechanical Engineering of the University of Notre Dame

Notre Dame, Indiana

May 2014

MATHEMATICAL MODEL AND EXPERIMENTAL DESIGN OF AN AIR-FILLED ALPHA STIRLING REFRIGERATOR

Abstract

by

Patrick K. McFarlane

Both a mathematical and physical model of a Stirling refrigerator is developed here. The mathematical model is for an alpha Stirling refrigerator with air as the working fluid and will be useful in optimizing the mechanical design of these machines. Two pistons cyclically compress and expand air while moving sinusoidally in separate chambers connected by a regenerator, thus creating a temperature difference across the system. A complete non-linear mathematical model of the machine, including air thermodynamics, and heat transfer from the walls, as well as heat transfer and fluid resistance in the regenerator, is developed. Non-dimensional groups are derived, and the mathematical model is numerically solved. The heat transfer and work are found for both chambers, and the coefficient of performance of each chamber is calculated. Important design parameters are varied and their effect on refrigerator performance determined. This sensitivity analysis, which shows what the significant parameters are, is a useful tool for the design of practical Stirling refrigeration systems.

The physical model consists of the design and experimental testing of a similar alpha Stirling refrigerator with air as the working fluid and where the conventional piston-cylinder assemblies are replaced by flexible chambers. The two chambers are cyclically compressed by pneumatic actuators resulting in airflow through the regenerator and in a net temperature difference between the chambers. The experimental

setup is used to investigate the performance of the refrigerator under different operating conditions with particular attention to actuation frequency, external pressure amplitude, and phase angles between the two inputs. The time constant of the temperature difference between the two chambers is determined, and this difference is measured as a function of the system parameters. The test results show that the operation is very robust and allows good performance even in the case of modulated input. This work suggests that mechanical to thermal energy conversion devices based on the Stirling principle can be successfully integrated into human-motion driven flexible structures to exploit the mechanical energy associated with mechanical deformations. The recommendations for future research on this topic indicate the need for further physical testing on a smaller, wearable Stirling refrigerator.

CONTENTS

FIGURES

TABLES

ACKNOWLEDGMENTS

I gratefully acknowledge the support of Mr. Christopher G. Slatt and Mrs. Jeanine Slatt through The Vincent P. Slatt Fellowship for Undergraduate Research in Energy Systems and Processes for this project. I also thank Dr. Rafael Chávez-Martínez for measurement of the thermocouple time constant for the physical model and Kevin Peters for help with LabVIEW. Thank you to Jonathan Suire for constructing the physical model of the Stirling refrigerator. I am also extremely grateful to Professor Fabio Semperlotti and Professor Mihir Sen for their guidance and support throughout my research. Lastly, I want to thank my parents and family for always being there for me.

This research also lead to a journal publication on the mathematical model in the Journal of Applied Physics[1]. A second manuscript on the physical model has been sent to the same journal, and is currently under review at the time of this thesis submission[2].

CHAPTER 1

INTRODUCTION

In recent years, alternative energy sources have garnered considerable interest. The need for energy permeates nearly all aspects of daily life. However, all of this energy consumption comes at a cost, economically and environmentally. Also, some energy sources are not available in certain areas or situations. A low-cost energy source available when traditional energy sources are absent or depleted is valuable. Energy harvesting is the utilization of small amounts of ambient energy, which would otherwise go to waste, into a usable form of energy. By taking advantage of this "free" energy, devices can become efficient or even self-sufficient. This type of energy conversion is not to be confused with energy generation, which uses storable fuels to generate power on a large scale, such as an internal combustion engine or power plant. Currently, the relatively small amount of energy harnessed limits the potential applications of energy harvesting devices. Different sources of energy can be used for energy harvesting, depending on the technique used.

This work analyzes a specific application of energy harvesting that converts a mechanical energy input into thermal energy, or thermocompressive energy harvesting. This application is the Stirling refrigerator. Refrigerators use mechanical energy to drive heat from a low temperature source to a high temperature sink, and the Stirling machine is one of these that can be used for this purpose. Though such a device was proposed in the mid-1800's [3], Stirling refrigerators still have limited commercial use for household refrigeration and air-conditioning because of the better performance and convenience of conventional vapor-compression and absorption ma-

chines. Smaller Stirling machines are mostly used to cool computer parts. For these reasons, the Stirling machine may be more useful as an energy harvesting device. The mechanical input to the Stirling machine could be an ambient vibration or force, and the resulting temperature difference could be used to cool or heat for a given application. One such application of interest is obtaining mechanical energy from movement such as a walking or rocking motion to produce heat flow that provides a comfortable temperature for the user. Air-filled Stirling machines have an advantage in this type of application because of their simplicity.

The Stirling machine consists of an expansion space and compression space filled with the working fluid connected by a regenerator. The expansion space has a cold heat exchanger to exchange heat between the working fluid and the low temperature source. The compression space has a warm heat exchanger to exchange heat between the working fluid and the high temperature sink. The spaces are compressed or expanded by either two pistons or a piston and a displacer. The regenerator is an internal heat exchanger which stores heat transferred from the heated working fluid. As the cooled working fluid passes through the regenerator from the compression space, heat is transferred from the regenerator to the working fluid. This process creates a temperature difference across the Stirling refrigerator.

Although the Stirling machine does not operate with ideal cycles, the ideal Stirling cycle demonstrates the principles behind the Stirling machine. The ideal Stirling cycle begins with an isothermal expansion in the expansion space. The expansion space is kept at a constant temperature by absorbing heat from the low temperature source. The second step is an isochoric heat transfer as the heated working fluid from the expansion space passes through the regenerator, cooling the fluid. The third step is an isothermal compression of the working fluid in the compression space. The compression space is kept at a constant low temperature through the removal of heat to the high temperature sink. The last step is an isochoric heat transfer from the

regenerator to the cool fluid from the compression space. This completes the ideal Stirling cycle and returns the cycle to the first step of isothermal expansion of the working fluid.

There are three types of Stirling machines: alpha, beta, and gamma. Each type operates under the same Stirling cycle, but the internal configurations differ slightly. The alpha Stirling machine consists of two chambers separated by a regenerator. The alpha Stirling machine can be seen in Fig. 1.1. The beta Stirling machine differs

Figure 1.1. Alpha Stirling machine, where 1 is the expansion space with the cold heat exchanger, 2 is the compression space with the warm heat exchanger, and the connecting portion is the regenerator.

from the alpha type in that it consists of one piston and one displacer. Unlike the piston, the displacer is not externally driven by a mechanical input. The displacer is positioned so as to separate the expansion space from the compression space. The piston motion creates pressure oscillations which dictate the motion of the displacer. The beta Stirling machine has one chamber separated into the compression and expansion spaces by the displacer, while the alpha Stirling machine has two separate chambers. The beta Stirling machine can be seen in Fig. 1.2. The gamma Stirling machine is similar to the beta Stirling machine, but it consists of two chambers instead of one. This allows for a larger separation of the heat exchangers and the

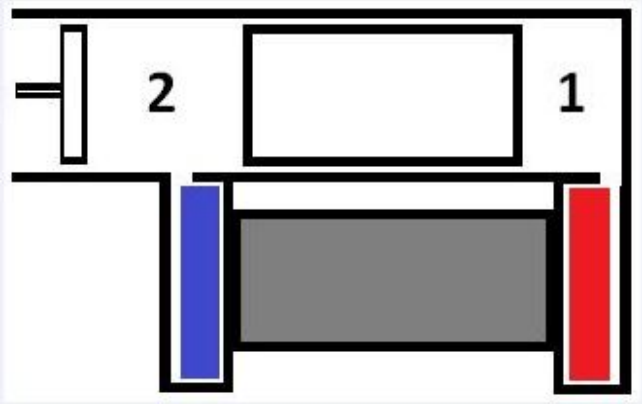

Figure 1.2. Beta Stirling machine, where 1 is the expansion space with the cold heat exchanger, 2 is the compression space with the warm heat exchanger, and the displacer separates the two spaces.

expansion and compression spaces. The gamma Stirling machine can be seen in Fig. 1.3.

This work examines both a mathematical and a physical model of an air-filled alpha Stirling refrigerator. The mathematical model is derived from first principles for each section of the refrigerator, while allowing for heat transfer in each section at all times during the cycle. To study this model, the equations are solved numerically using a computer program. A sensitivity analysis is performed to indicate the more important parameters affecting performance of the refrigerator. The intention of this analysis is to guide the designer of a Stirling refrigerator as to which parameters affect performance more than others. The experimental section describes the design, construction, and testing of an air-filled alpha Stirling refrigerator with flexible chambers driven by pneumatic actuators. Although the physical model differs slightly from the mathematical model, the results from each section are analyzed and discussed. The purpose of both models is to demonstrate the viability of the Stirling refrigerator as an energy harvesting device. This work is organized as follows: Chapter 2 presents the mathematical model derivation, simulation, and analysis, Chapter 3 presents the

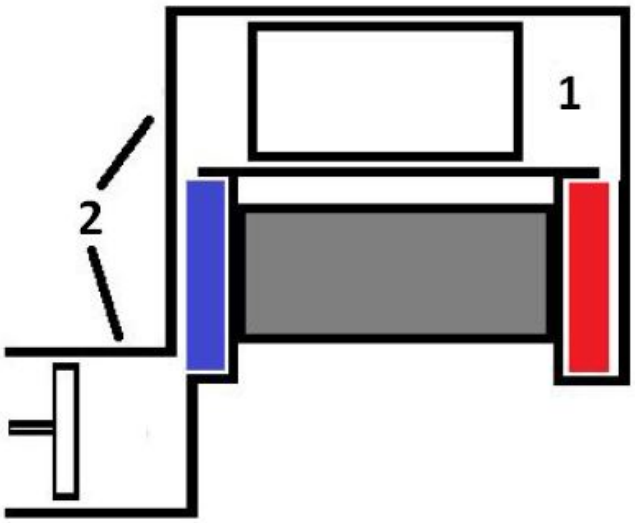

Figure 1.3. Gamma Stirling machine, where 1 is the expansion space with the cold heat exchanger, 2 is the compression space with the warm heat exchanger, and the displacer separates the two spaces.

experimental design and construction, Chapter 4 presents the results of the experimental testing, and Chapter 5 adds conclusions and recommendations based on this research.

CHAPTER 2

MATHEMATICAL MODEL

2.1 LITERATURE REVIEW

This literature review covers the relevant literature for mathematical models of Stirling refrigerators. Even though the operation of the Stirling refrigerator differs from that of the ideal Stirling cycle, some researchers rely on the latter for their studies[4, 5, 6]. Wu et al.[7] and Kaushik and Kumar[8] used a finite time thermodynamic analysis of Stirling machines. By assuming the ideal cycle partially or completely, any analysis of the refrigerator deviates from the actual physics occurring during operation. In their review, Chakravarthy et al.[9] classified the Stirling refrigerator as a periodic refrigeration system, which indicates that the pressure and flow rate in the refrigerator fluctuate periodically. Thombare and Verma[10] provided a thorough review of the work done on Stirling cycle-based machines. Although the review focused on engines, the analysis of the departure of Stirling machines from the ideal Stirling cycle remains relevant. Waele[11] provided a comprehensive overview of Stirling cryocoolers and other thermal machines. Tekin and Ataer[12] looked at improving the design of a V-type Stirling-cycle refrigerator in a previous model by Ataer and Karabulut[13] using a thermodynamic approach. Chen and Yan[14] developed a model for a Stirling refrigerator that investigated the effects of non-ideal regenerators. Erbay and Yavuz[15] took a more practical approach to the analysis of Stirling refrigerators by studying the cooling load per unit volume. Omari[16] compared the differences between the ideal and real Stirling cycles that occur in the

refrigerator, but lacked analysis of the affect of system parameters on performance.

The real cycle includes heat transfer in each section of the refrigerator during any part of the cycle, as well as a non-ideal regenerator. Including these physical processes is important because a more physically sound model provides the designer with a better estimate of how the refrigerator will perform under actual operating conditions. This work provides a more detailed and comprehensive model for Stirling refrigerators than previously published. By allowing for heat transfer throughout the entire system and duration of the cycle, the present analysis minimizes the simplifications made in previous derivations. It improves upon the model Chen and Yan[14] developed because they include isochoric and isothermal processes in the cycle. It also provides a deeper analysis of the factors that affect refrigerator performance compared to Tekin and Ataer[12], since they assumed the regenerator to be adiabatic. In addition, it improves upon the model of Erbay and Yavuz[15] because they included the isochoric processes of an ideal Stirling cycle.

In the following, the governing equations for each section of the refrigerator are developed. The derivations use the basic conservation laws, and also account for heat transfer in the cylinders and regenerator. The model is solved numerically for a number of cycles to remove the effect of the initial transients on the solution. The numerical results are presented to illustrate the performance of the machine, and design parameters that affect performance are derived and discussed.

2.2 MATHEMATICAL MODEL DERIVATION

The model is based on the following considerations: the working fluid is an ideal gas, air; there is no leakage of mass from the system; the input motion of the pistons is sinusoidal; the walls of the compression and expansion space are at a constant temperature. It is assumed that the heat generated by friction in the regenerator is negligible.

2.2.1 COMPRESSION AND EXPANSION SPACE EQUATIONS

Consider the Stirling refrigerator in Fig. 2.1. The chamber that extracts net heat from the surroundings will be referred to as the expansion space, and the chamber that releases net heat to the surroundings as the compression space. For convenience, variables associated with the former will have a subscript 1, while those associated with the latter will have a subscript 2. The prescribed motions of the pistons are

$$x_1 = x_{0,1} + \hat{x}_1 \sin(\omega t), \tag{2.1a}$$

$$x_2 = x_{0,2} + \hat{x}_2 \sin(\omega t + \phi). \tag{2.1b}$$

The pistons move with a frequency ω, an amplitude $\hat{x}_i$ and central position $x_{0,i}$ for the chamber i piston. The phase shift ϕ in the motion of the two chamber pistons results in the reciprocating flow between the two chambers; ϕ will turn out to be a critical parameter for the proper operation of the machine.

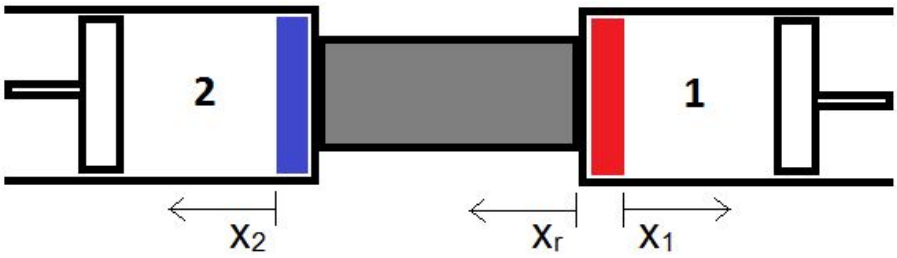

Figure 2.1. Alpha Stirling refrigerator, where 1 is the expansion space with the cold heat exchanger, 2 is the compression space with the warm heat exchanger, and the connecting portion is the regenerator. The arrows point in the positive direction for each coordinate.

Energy balance on chamber i gives

$$\begin{aligned} \underbrace{c_v M_i \frac{dT_i}{dt}}_{1} &= \underbrace{h_i \pi D_i x_i (T_{w,i} - T_i)}_{2} \\ &+ \underbrace{[c_v \dot{m}_{in}(T_{in} - T_i) + \frac{P_{in}}{\rho_{in}} \dot{m}_{in}]}_{3} \\ &- \underbrace{[c_v \dot{m}_{out}(T_{out} - T_i) + \frac{P_{out}}{\rho_{out}} \dot{m}_{out}]}_{4} - \underbrace{P_i \frac{dV_i}{dt}}_{5} \end{aligned} \tag{2.2}$$

Term 1 represents the rate of change of the temperature of the air in a chamber with respect to time t, where M_i and T_i are the mass and temperature of the air, respectively, and c_v is the heat capacity per unit mass of air at constant volume. Term 2 is the heat transfer from the walls of the chamber to the air, where h_i is the convective heat transfer coefficient, D_i is the piston diameter, x_i is the distance from the regenerator, and $T_{w,i}$ is the temperature of the chamber wall. Term 3 represents the enthalpy of the incoming flow to the chamber, where $\dot{m}_{in}$ is the mass flow rate into the chamber, T_{in} is the temperature of the incoming flow, P_{in} is the pressure at the inlet, and ρ_{in} is the density of the incoming flow. Term 4 represents the enthalpy of the outgoing flow, where $\dot{m}_{out}$ is the mass flow rate out of the chamber, T_{out} is the temperature of the outgoing flow, P_{out} is the pressure at the outlet, and ρ_{out} is the density of the outgoing flow. Term 5 is the work done by the air on the piston, where P_i is the pressure on the piston and V_i is the volume of the air in the chamber.

Eq. (2.2) can be applied to the two chambers for one-dimensional airflow in either direction, i.e. from chamber 1 to chamber 2 or vice versa. For incoming flow from the regenerator, Term 4 becomes zero, while for outgoing flow to the regenerator, Term 3 becomes zero. This is a result of the physics of the airflow.

Assuming ideal gas behavior for the air,

$$P_i x_i \frac{\pi D_i^2}{4} = M_i R T_i, \tag{2.3}$$

where R is the specific gas constant for air. Because of air flow through the regenerator, the mass of the air in each chamber is not constant. The rate of change of this mass is

$$\frac{dM_1}{dt} = -\frac{dM_2}{dt} = -\rho u \frac{\pi D_r^2}{4} = -\dot{m}, \tag{2.4}$$

where u is the velocity of the flow in the regenerator, D_r is the regenerator tube diameter, and ρ is the density of the air in the regenerator. Based on Fig. 2.1, u is positive in the direction from chamber 1 to chamber 2.

2.2.2 REGENERATOR EQUATIONS

Similar equations can be derived for the regenerator section. Consider the regenerator as a metal tube of length L_r, and diameter D_r. Energy balances for the air in the regenerator, whose temperature $T_r(x_r, t)$ varies with space and time, as well as the regenerator wall, whose temperature $T_w(t)$ varies only with time, are

$$\rho c_p \frac{\pi D_r^2}{4} \frac{\partial T_r}{\partial t} + \dot{m} c_p \frac{\partial T_r}{\partial x_r} = h_r \pi D_r (T_w - T_r) + q_f, \tag{2.5}$$

$$M_w c_w \frac{dT_w}{dt} = -\int_0^{L_r} h_r \pi D_r (T_w - T_r) dx_r, \tag{2.6}$$

where ρ is the density of the air in the regenerator, c_p is the specific heat per unit mass of air at constant pressure, and h_r is the convective heat transfer coefficient in the regenerator. Although q_f is the heat generated by friction in the regenerator, we take it to be negligible when compared to the heat transfer with the regenerator wall. M_w is the mass of the regenerator wall, c_w is the specific heat per unit mass of the

metal, and x_r is a location along the regenerator from chamber 1 to chamber 2.

The velocity of the air in the regenerator depends on the pressure difference between the chambers as

$$\dot{m} = \begin{cases} \sqrt{\dfrac{\rho\pi D_r^5(P_1 - P_2)}{32 L_r f}} & \text{for } P_1 \geq P_2 \\ -\sqrt{\dfrac{\rho\pi D_r^5(P_2 - P_1)}{32 L_r f}} & \text{for } P_2 > P_1 \end{cases} \tag{2.7}$$

where f is the friction factor. The inertia of the air has been neglected.

2.2.3 NONDIMENSIONAL EQUATIONS

To nondimensionalize the equations, we define

$$\begin{gathered} t^* = \frac{t\omega}{2\pi}, x_i^* = \frac{x_i}{\hat{x}_1}, v_i^* = \frac{v_i}{\omega \hat{x}_i}, T_i^* = \frac{T_i - \bar{T}}{\Delta T}, \\ P_i^* = \frac{P_i - \bar{P}}{\Delta P}, \dot{m}^* = \frac{\dot{m}}{\hat{M}\omega}, M_i^* = \frac{M_i}{\hat{M}}, x_r^* = \frac{x_r}{L_r}, \\ T_r^* = \frac{T_r - \bar{T}}{\Delta T}, T_{w,i}^* = \frac{T_{w,i} - \bar{T}}{\Delta T} \end{gathered} \tag{2.8}$$

where the starred variables are non-dimensional. Also

$$\Delta T = \frac{\bar{T}(V^{\gamma-1} - V_{min}^{\gamma-1})}{V_{min}^{\gamma-1}}, \tag{2.9}$$

$$\Delta P = \frac{\bar{P}(V^{\gamma} - V_{min}^{\gamma})}{V_{min}^{\gamma}}, \tag{2.10}$$

where $\gamma = c_p/c_v$, $\bar{T}$ is the starting air temperature, and $\bar{P}$ is the starting air pressure. ΔT and ΔP are characteristic temperature and pressure rises, respectively, if the air were to be compressed adiabatically to its minimum volume.

The following nondimensional groups

$$\Pi_1 = \phi, \Pi_2 = f, \Pi_3 = \frac{c_p}{c_v}, \Pi_4 = \frac{D_i}{D_r},$$
$$\Pi_5 = \frac{\hat{M}}{M_w}, \Pi_6 = \frac{x_{0,i}}{L_r}, \Pi_7 = \frac{c_v}{c_w}, \Pi_8 = \frac{h_i}{h_r},$$
$$\Pi_9 = \frac{\hat{x}_i}{x_{0,i}}, \Pi_{10} = \frac{\hat{x}_i}{D_i}, \Pi_{11} = \frac{h_i}{c_v \rho D_i \omega}, \Pi_{12} = \frac{\hat{M}}{\rho D_i^3},$$
$$\Pi_{13} = \frac{\Delta P}{\bar{P}}, \Pi_{14} = \frac{\Delta T}{\bar{T}}, \Pi_{15} = \frac{\Delta P}{\rho c_v \Delta T}, \Pi_{16} = \frac{\rho R \Delta T}{\Delta P},$$
$$\Pi_{17} = \frac{\rho \pi^2 D_r^5 \Delta P}{32 L_r f \hat{M}^2 \omega^2} \tag{2.11}$$

appear in the model, where $\hat{M}$ is the total air mass in the refrigerator.

The governing equations become

$$x_1^* = \frac{1}{\Pi_9} + \sin(2\pi t^*) \tag{2.12a}$$

$$x_2^* = \frac{1}{\Pi_9} + \sin(2\pi t^* + \Pi_1) \tag{2.12b}$$

$$\begin{aligned} M_i^* \frac{dT_i^*}{dt^*} &= 2\pi^2 \frac{\Pi_{10}\Pi_{11}}{\Pi_{12}} x_i^* (T_{w,i}^* - T_i^*) \\ &+ [2\pi \dot{m}_{in}^* (T_{in}^* - T_i^*) + 2\pi \dot{m}_{in}^* (\Pi_{15} P_{in}^* + \frac{\Pi_{15}}{\Pi_{13}})] \\ &- [2\pi \dot{m}_{out}^* (T_{out}^* - T_i^*) + 2\pi \dot{m}_{out}^* (\Pi_{15} P_{out}^* + \frac{\Pi_{15}}{\Pi_{13}})] \\ &- \frac{\pi}{4} (\frac{\Pi_{15}\Pi_{10}}{\Pi_{12}} P_i^* + \frac{\Pi_{15}\Pi_{10}}{\Pi_{13}\Pi_{12}}) \frac{dx_i^*}{dt^*} \end{aligned} \tag{2.12c}$$

$$(P_i^* + \frac{1}{\Pi_{13}}) x_i^* = \frac{4}{\pi} \frac{\Pi_{16}\Pi_{12}}{\Pi_{10}\Pi_{14}} M_i^* + \frac{4}{\pi} \frac{\Pi_{16}\Pi_{12}}{\Pi_{10}} M_i^* T_i^* \tag{2.12d}$$

$$\frac{d\dot{M}_1^*}{dt^*} = -\frac{d\dot{M}_2^*}{dt^*} = -2\pi \dot{m}^* \tag{2.12e}$$

$$\begin{aligned} &\frac{1}{8\pi} \frac{\Pi_3\Pi_8}{\Pi_{11}\Pi_4} \frac{\partial T_r^*}{\partial t^*} + \frac{1}{\pi} \frac{\Pi_6\Pi_9\Pi_4\Pi_8\Pi_3\Pi_{12}}{\Pi_{10}\Pi_{11}} \dot{m}^* \frac{\partial T_r^*}{\partial x_r^*} \\ &\qquad = (T_w^* - T_r^*) + q_f^* \end{aligned} \tag{2.12f}$$

$$\frac{dT_w^*}{dt^*} = -2\pi^2 \frac{\Pi_{10}\Pi_{11}\Pi_7\Pi_5}{\Pi_6\Pi_9\Pi_4\Pi_8\Pi_{12}} \int_0^1 (T_w^* - T_r^*) dx_r^* \tag{2.12g}$$

$$\dot{m}^* = \begin{cases} \Pi_{17}^{1/2} \sqrt{P_1^* - P_2^*} & \text{for } P_1^* \geq P_2^* \\ -\Pi_{17}^{1/2} \sqrt{P_2^* - P_1^*} & \text{for } P_2^* > P_1^* \end{cases} \tag{2.12h}$$

2.2.4 SOLUTION PROCEDURE

The equations are solved numerically. Time and spatial steps of 0.0001 and 0.001, respectively, were used to ensure numerical convergence to the solution.

The first-order partial differential equation is solved using the method of characteristics. Equation 2.6 can be reduced to

$$\frac{\partial T_r}{\partial t} + u \frac{\partial T_r}{\partial x_r} = H(T_w - T_r), \tag{2.13}$$

where $H = 4h_r/\rho c_p D_r$. The method of characteristics reduces this to two ordinary differential equations given by the relations

$$\frac{dt}{1} = \frac{x_r}{u} = \frac{dT_r}{H(T_w - T_r)}. \tag{2.14}$$

The first relation gives

$$\frac{dx_r}{dt} = u, \tag{2.15}$$

which is simply an expression for the velocity of the fluid along the regenerator. The second relation gives

$$\frac{dT_r}{dx_r} = \frac{H}{u}(T_w - T_r), \tag{2.16}$$

or

$$\frac{dT_r}{dt} = H(T_w - T_r). \tag{2.17}$$

The differential equation for T_r used depends on u. If the flow has not reached a location x_r along the regenerator, the temperature at that point only depends on the heat transfer from the regenerator walls, so Equation 2.17 is used. If the flow has reached a location x_r, the temperature at that point depends on the flow from the chamber, so Equation 2.16 is used. The computer code attached in the Appendix explains the numerical solution of these and all equations, as well as the switching between characteristics depending on the nature of the flow.

The simulation uses the physical parameters of the refrigerator given in Table 2.1. The initial pressures are taken to be 1 atm, and all initial temperatures 300 K. The convective heat transfer coefficient for each section of the refrigerator is assumed to be in the range for gases under forced convection. The choice of this convective heat transfer coefficient will be analyzed in the sensitivity analysis. Because of the low Reynolds number in the regenerator, the friction factor corresponds to that for laminar flow. The temperature of the chamber walls remains constant at 300 K, so

any heat transfer to or from the walls is considered to be with a cold reservoir for chamber 1 and with a hot reservoir for chamber 2.

TABLE 2.1

Physical parameters

Parameter(s)	Value
Piston diameter D	50 mm
Regenerator pipe diameter D_r	5 mm
Regenerator pipe length L_r	100 mm
Convection coefficients h_r, h_1, h_2	100 W/(m^2 K)
Frequency of piston motion ω	1.5 rad/s
Phase angle ϕ	$\frac{\pi}{2}$ rad
Piston amplitude $\hat{x}_1$, $\hat{x}_2$	50 mm
Piston center position $x_{0,1}$, $x_{0,2}$	100 mm (from regenerator)
Regenerator friction factor f	0.1
Regenerator mass M_w	1 kg

2.3 RESULTS

2.3.1 REFRIGERATION CYCLE

The model was used to simulate the performance of the Stirling refrigerator over two cycles. The results show the second cycle of operation because the first contains

transient effects caused by the initial conditions, which decay by the second.

Fig. 2.2 shows the P-V diagram of the expansion space. This plot shows the refrigeration cycle of chamber 1. This curve can be seen to be quite different from that of the ideal cycle.

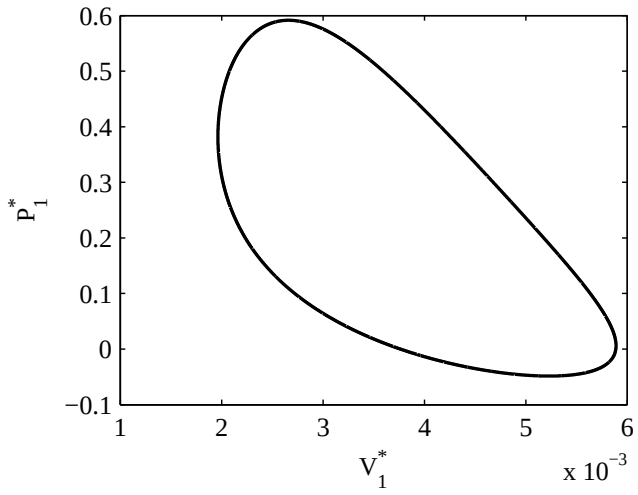

Figure 2.2. Pressure-volume diagram for chamber 1 over a cycle.

Fig. 2.3 illustrates the temperature, pressure, and mass of the air in chamber 1 along with its piston motion. Fig. 2.4 has the temperature, pressure, and mass of the air in chamber 2 along with its piston motion. Comparing the two figures, a temperature difference between the two chambers is seen to develop at half of the cycle duration, where the temperature of the chamber 1 air drops as the temperature of the chamber 2 air rises. This causes the chamber 1 walls to transfer heat to the air in that chamber, cooling the walls. Also, heat is transferred from the hotter air in chamber 2 to the walls, heating them.

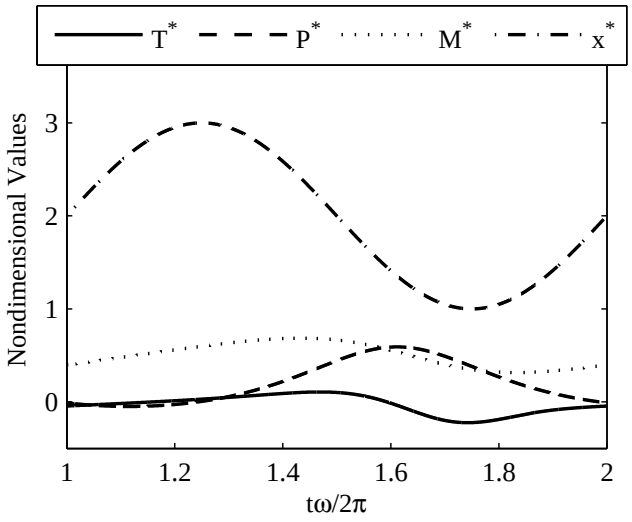

Figure 2.3. Air temperature T_1^* (solid -), pressure P_1^* (dashed –), and mass M_1^* (dotted ..) in chamber 1 over a cycle. This also shows the chamber 1 piston motion x_1^* (dash-dot -.).

The pressure difference between the chambers enables the flow of the air through the regenerator, which can be seen in Fig. 2.5. The phase shift in the sinusoidal motion of the pistons causes the pressure difference between the two chambers and thus mass fluctuations in each chamber. This mass flow between chambers is an important aspect of the Stirling refrigerator because it couples the two chambers together. The mass difference between the chambers also affects the heat transfer in each chamber.

To evaluate the refrigerator performance, the heat transfer and work input

$$Q_1 = \int_0^t h_1 \pi D_1 x_1 (T_{w,1} - T_1) dt \tag{2.18}$$

$$Q_2 = \int_0^t h_2 \pi D_2 x_2 (T_{w,2} - T_2) dt \tag{2.19}$$

$$W = \int_0^t P_1 \frac{dV_1}{dt} dt + \int_0^{\frac{t\omega}{2\pi}} P_2 \frac{dV_2}{dt} dt \tag{2.20}$$

must be found. Fig. 2.6 shows the heat transfer at every instant throughout the

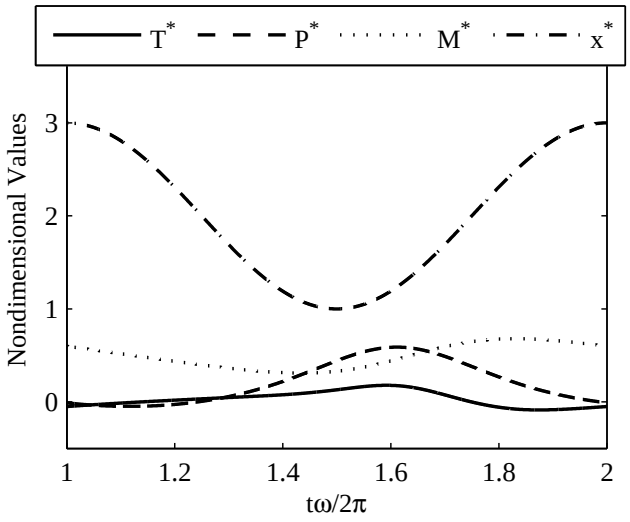

Figure 2.4. Air temperature T_2^* (solid -), pressure P_2^* (dashed –), and mass M_2^* (dotted ..) in chamber 2 over a cycle. This also shows the chamber 2 piston motion x_2^* (dash-dot -.).

cycle.

Over a cycle, the coefficient of performance is the ratio of the net heat transfer between the chamber air and the chamber walls to the total work input to the refrigerator, so that

$$COP_1 = \frac{Q_1}{W} \tag{2.21a}$$

$$COP_2 = \frac{Q_2}{W} \tag{2.21b}$$

where COP_1 is the coefficient of performance of a refrigerator because chamber 1 provides the cooling, and COP_2 is that of a heat pump because chamber 2 provides the heating. Because this Stirling refrigerator is not ideal, there is unwanted heat transfer to the cold reservoir (chamber 1 walls) and unwanted heat transfer from the hot reservoir (chamber 2 walls), as seen in Fig. 2.6. Table 2.2 shows results relevant to the performance of this Stirling refrigerator.

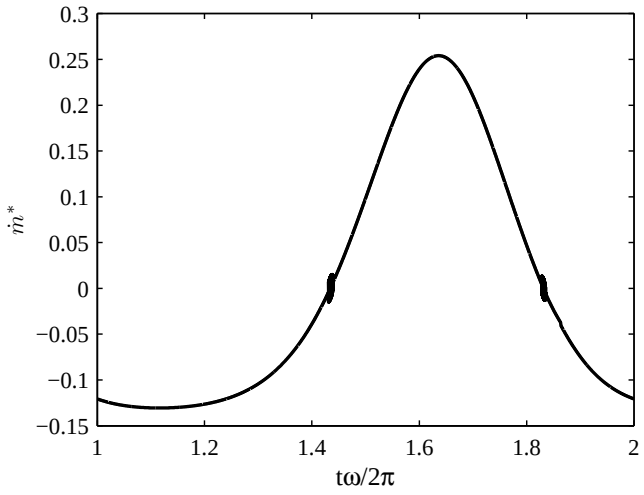

Figure 2.5. Mass flow rate $\dot{m}^*$ in the regenerator over the cycle. The slight mass flow rate fluctuation around 0 is numerical due to the change of sign of the velocity. The equation switches between the two cases of Eq. (2.7) when the sign changes, resulting in this discontinuity.

2.4 SENSITIVITY ANALYSIS

To study the affect of the refrigerator parameters on design, our focus will be on parameters that the designer can choose to alter. The sensitivity analysis varies the piston amplitude $\hat{x}_i$, piston center position $x_{0,i}$, phase angle ϕ, piston frequency ω, and regenerator diameter D_r. Although harder to change, the analysis also varies the convective heat transfer coefficient. Each parameter is varied while holding all others constant to isolate the effect of that parameter only.

To see how the heat transfer changes, we define a nondimensional heat transfer term Q_i^*, which is

$$Q_i^* = \int_1^2 \frac{h_i D_i \hat{x}_i}{h_o D_o \hat{x}_{0,i}} x_1^* (T_w^* - T_i^*) \frac{2\pi dt^*}{\omega t_f}. \tag{2.22}$$

h_o, D_o, $\hat{x}_{0,i}$, and t_f are all of the values used in the simulation described in Table 2.1 for the convective heat transfer coefficient, piston diameter, and piston amplitude. t_f is the time it takes to run a cycle of that refrigerator.

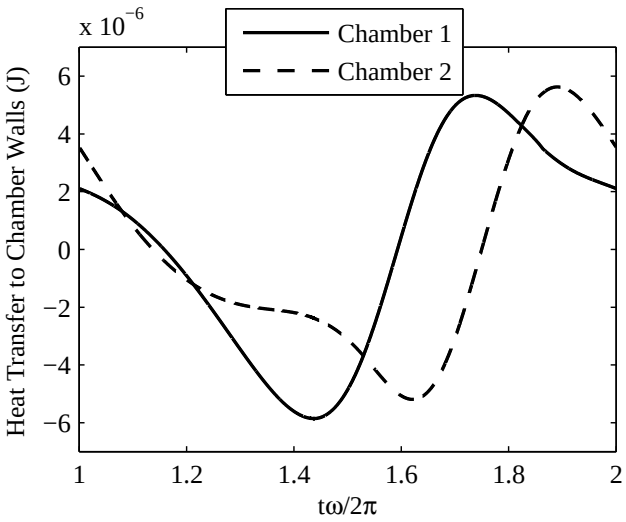

Figure 2.6. Heat transfer Q^* throughout the cycle in each chamber. Heat transfer from the walls to the air is positive, so chamber 1 (expansion space) has a net cooling effect on the chamber wall, while chamber 2 (compression space) has a net heating effect on the chamber wall.

Fig. 2.7 shows the effect of the piston amplitude. Increasing the amplitude of both of the pistons' motion increases the heat transfer to chamber 1 and the heat transfer from chamber 2. This effect is confirmed by the amplitude term appearing in Q_i^*.

Fig. 2.8 shows the effect of the piston center position. The increase of that distance increases the volume of each chamber. Because the other parameters are held constant, two things occur. First, the piston amplitude remains constant, so the air is compressed and expanded less due to the increased volume; this causes the trend seen in Fig. 2.8 as the cooling of chamber 1 and the heating of chamber 2 decreases. Second, the mass of air in the refrigerator remains constant, so the density in the refrigerator drops with increasing center position. Fig. 2.8 shows the trend that occurs with increasing center position, especially near the nominal value of 0.1 m because the density is close to the simulation above.

Fig. 2.9 shows the effect of the phase angle in the motion of the chamber 2

TABLE 2.2

Results from one cycle of a Stirling refrigerator

Variable	Value
Mean chamber 1 air temperature	297.1689 K
Mean chamber 2 air temperature	303.1228 K
Heat Transfer to chamber 1 from walls	1.9037 J
Heat Transfer from chamber 2 to walls	4.3466 J
COP_1	1.0706
COP_2	2.4446

piston. Q_1^* peaks around 70° which indicates that a phase angle of 90° is not optimal for this Stirling refrigerator. Fig. 2.9 agrees with the trend given by Tekin[12], but it also expands the trend by exploring 360° of phase difference. The symmetry of this figure signals that, when the phase angle is 180° or greater, the chambers switch roles. When ϕ is larger than 180°, chamber 2 provides the cooling power, while chamber 1 provides the heating power. The lack of cooling around 0 and 360° is attributed to the low mass flow rate due to the small difference between the motion of the pistons. Here, the chambers almost become two separate systems because the mass flow approaches zero. The lack of cooling around 180° can be attributed to the particular motion of the pistons as the pistons have opposite motions. One piston moves towards the regenerator as the other moves away, so the machine is simply pushing the air around the refrigerator without much compression or expansion.

Fig. 2.10 shows the effect of the frequency of the piston motion. The heat transfer increases with frequency, which also agrees with Tekin[12] who analyzes much higher frequencies. The faster compression and expansion leads to larger temperature differences.

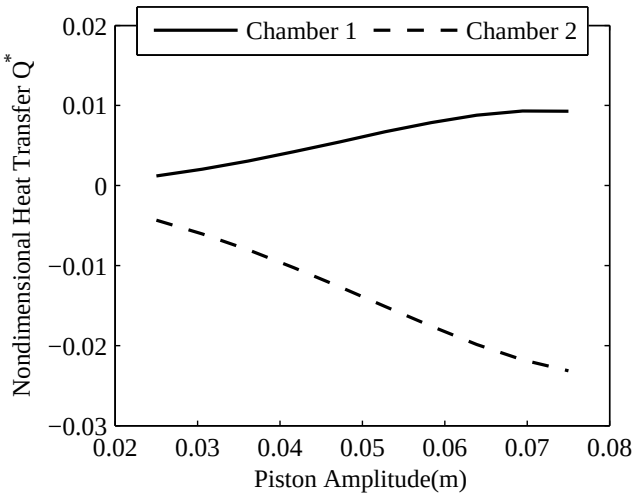

Figure 2.7. Heat transfer versus piston amplitude for both chambers. Notice how Q_i^* levels off as the amplitude gets large. This is due to the center position of each piston remaining at 0.1 m. As the amplitude approaches this value, the heat transfer levels off because the amount the air can be compressed is decreased.

Fig. 2.11 shows the effect of the regenerator diameter. Similar to varying the piston center position, the mass of the air in the refrigerator remains constant. Therefore, the predictions of the refrigerator performance at the ends of the range of values tested is affected by the high or low air density. However, the figure does show the trend that increasing the regenerator diameter increases the heat transfer in both chambers. This is due to the increased contact area in the regenerator, so the air can recover more heat from the wall or transfer more heat to the wall, increasing regenerator efficiency.

Fig. 2.12 shows the variation of heat transfer with convective heat transfer coefficients. For this analysis, the heat transfer coefficient is the same in both chambers and in the regenerator. The slight dip in heat transfer at the low end of the heat transfer coefficient values can be attributed to the regenerator effectiveness. If the heat transfer coefficient in the refrigerator is too low, the regenerator lacks efficiency

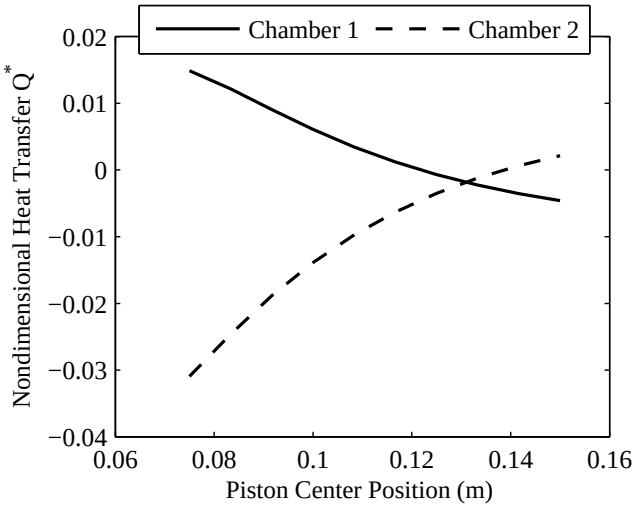

Figure 2.8. Heat transfer versus piston center position for both chambers. The behavior at either end of this graph is due to the high air density at small piston center position or low density air at large piston center position.

and the heat transfer declines. However, as the heat transfer coefficient increases after this dip, the heat transfer slightly increases. This plot supports the choice for a constant heat transfer coefficient in this range for the refrigeration cycle analysis of Table 2.1. Increases in the heat transfer coefficient correspond to a roughly constant relationship with the nondimensional heat transfer.

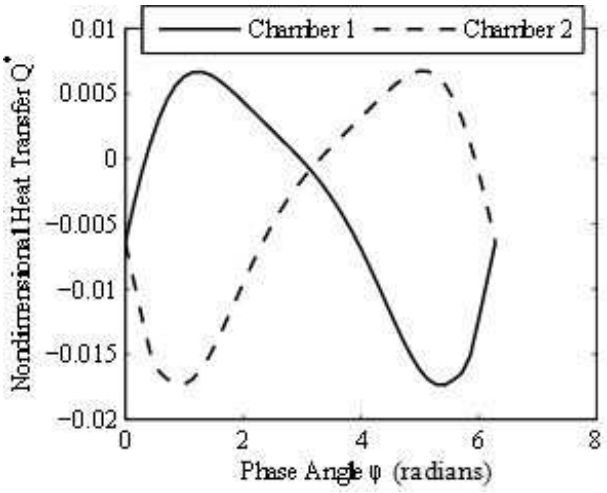

Figure 2.9. Heat transfer versus phase angle for both chambers. The symmetry of this plot about 180° (2π rad) shows that, when the heat exchangers are modeled as the chamber walls and the chamber walls are at the same temperature, the chambers switch heating and cooling roles.

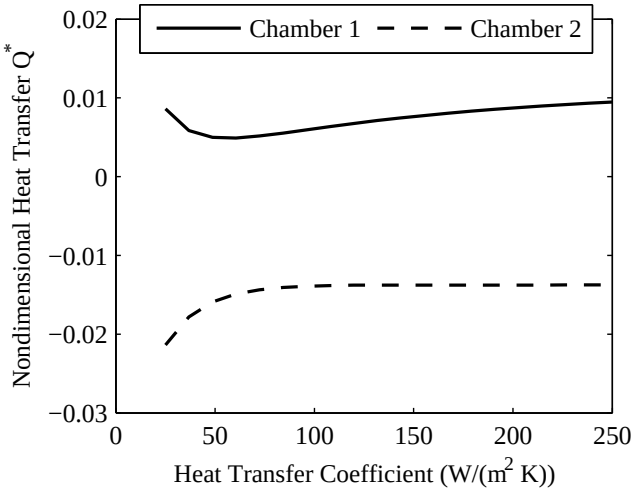

Figure 2.12. Heat transfer versus convective heat transfer coefficient for both chambers. This heat transfer coefficient corresponds to each chamber and the regenerator. Because the model allows for a net heat transfer between the air and the chamber walls, the net heat transfer only slightly changes with increasing heat transfer coefficient.

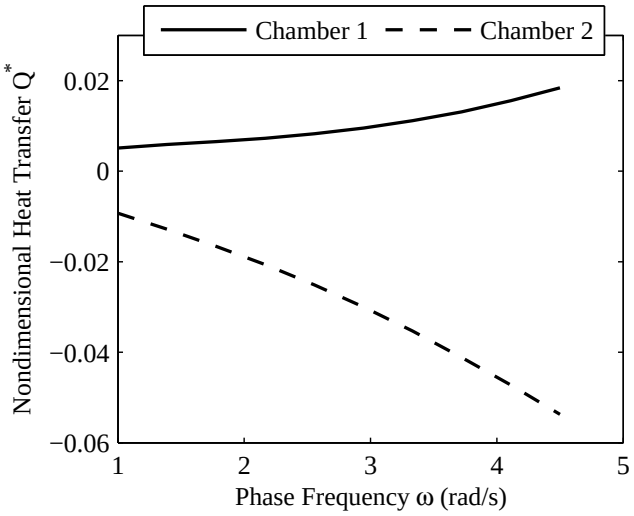

Figure 2.10. Heat transfer versus the frequency of piston motion for both chambers. The increase in heat transfer with increasing frequency is due to the faster compression and expansion, which creates a larger temperature difference across the refrigerator.

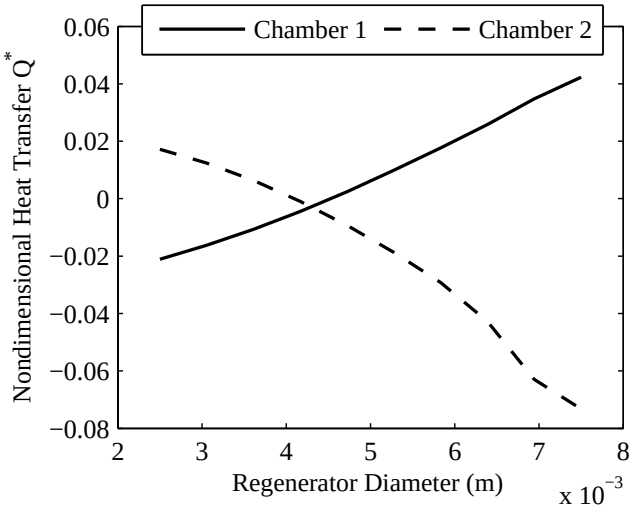

Figure 2.11. Heat transfer versus regenerator diameter for both chambers. This shows that increasing regenerator diameter increases regenerator efficiency, which increases the heat transfer in both chambers as well.

CHAPTER 3

EXPERIMENTAL CONSTRUCTION/SETUP

3.1 INTRODUCTION

This literature review covers the relevant literature for experiments involving Stirling refrigerators. Stirling refrigerators have been widely used in low-temperature applications like cryocooling [11], and there are also similar devices such as the Philips, Solvay, Little, Vuilleumier, Ericsson, pulse tube, and thermoacoustic refrigerators [17, 18, 9]. These mostly operate with motor-driven input and a piston-cylinder arrangement, and often operate at higher frequencies in order to cool as much as possible. The machines are usually run in the steady state, and that has been the main interest in previous studies.

Though there has been much done by many interested parties, there are only a few experiments reported in the peer-reviewed literature on Stirling refrigerators specifically. Osorio et al. [19] proposed a series of experiments with the small MicroStar K535 Stirling refrigerator as a didactic tool for teaching about cryogenics. Ki and Jeong [20] developed a step-by-step design for a Stirling pulse tube cryocooler which includes both the mathematical model and experimental verification. Antao and Farouk [21] performed numerical and experimental testing on their cryogenic pulse tube refrigerator. Luo et al. [22] constructed a thermoacoustic Stirling cryocooler driven by a thermoacoustic Stirling engine. Sun et al. [23] built and tested a prototype of a Stirling refrigerator for domestic refrigeration. There has been less emphasis on room-temperature Stirling refrigeration. He et al. [24] introduced a

hybrid refrigeration system that combined a magnetic with a Stirling refrigerator. Tang et al. [25] constructed a room-temperature Stirling refrigerator operating at high pressure to examine the oscillating flow.

The present research is motivated by a need to explore aspects that, although not very crucial for other applications, are of great importance for human-powered energy harvesting devices. The main aspects are summarized as follows:

1. The use of pressure-driven flexible chambers instead of piston-in-cylinder arrangements, since the former can be incorporated into wearable devices that can be powered by human-motion. The volume displacement in such a chamber is not prescribed by the known rotation of a motor and the related motion of a connecting rod, but is due indirectly to the difference between an applied outside pressure and the inside pressure. Thus, a major consequence of this design is that the flow of the working fluid within the machine is not *a priori* known, but is a function of the operation of the machine.

2. The use of thermal operating conditions close to what would be encountered in practical applications must be further investigated. In particular, the effect of small temperature differences, around 5° C, and low operating frequencies, around 1 Hz, on the overall performance of the refrigerator must be established.

3. The knowledge of the temperature differences that can be experimentally achieved as well as the characteristic time constant of the process are also of importance to evaluate the feasibility of human-powered devices. Devices with large time constants will not be useful in energy harvesting applications.

4. The effect of parameters such as phase angle difference between the two chambers and the amplitude of driving pressures is also significant. Unlike motor-driven machines, human-actuated devices will probably have a wide variation in these parameters during operation, as well as have aperiodic or modulated inputs.

To date, there are little or no reliable experimental data available in the areas mentioned. The experimental characterization of Stirling devices, with particular attention on the dependence of performance on these functional parameters, is key to bringing the Stirling machine closer to implementation in practical applications. In the following, the design and experimental testing of a Stirling refrigerator built using pressure-driven flexible chambers is described. The experiments explore the dependence of device performance on the above mentioned parameters.

3.2 EXPERIMENTAL SETUP AND TESTING PROCEDURE

From a general perspective, the Stirling refrigerator consists of two chambers connected by a regenerator. The chambers allow for the expansion and compression of the working fluid at the same frequency but at different phases, while the regenerator acts as a thermal reservoir to alternately extract and provide heat to the fluid. While conventional Stirling machines described in literature use a piston-cylinder assembly to do work on the working fluid, the proposed design uses flexible air-filled chambers that can be compressed by applying an external pressure. Thus, the amplitude of the volume change in each chamber is not fixed but is determined by the operating conditions. The main constitutive elements of this refrigerator design are described below. Fig. 3.1 shows a schematic of the Stirling refrigerator with flexible chambers.

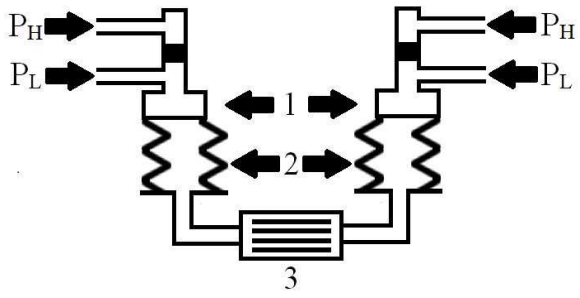

Figure 3.1. Schematic of Stirling refrigerator; (1), (2) and (3) indicate two pneumatic actuators, two flexible chambers, and regenerator, respectively. P_L is kept at a constant low pressure, while P_H is switched on and off with valves according to a pulse-shaped input signal. This provides the compression and expansion of the chamber.

3.2.1 DESIGN OF SETUP

Fig. 3.2 shows the actual experimental setup that was built. Pressurized air from the building is used as a source of air. There are two air lines that can be set to different pressures, one at a high pressure P_H, and the other at a low P_L. Each line goes to a double-acting pneumatic actuator (Clippard Minimatic, marked as (1) in Fig. 3.2) that provides the force that compresses the flexible chambers. Each actuator is connected to both the high and low pressure air that can be individually controlled to set specific pressure conditions to control the actuation. The low pressure air is connected to the bottom of the actuator, while the high pressure air is connected to the top of the actuator. The low pressure air is always on, while the high pressure air is switched on and off periodically by using computer-controlled electronic valves (Clippard ETN-3M-24), which are not shown in Figs. 3.1 and 3.2. The actuators compress the flexible chambers when the valves providing high pressure are open, and expand when they are closed. The pressure differences control the actuation force applied to the chambers and the change in volume therein.

The flexible chambers are off-the-shelf air springs (Goodyear 1B5-500, (2) in Fig. 3.2) that are normally used in motor vehicles. The chambers are connected to the regenerator by a thermally insulated polyurethane tube. The regenerator ((3) in Fig. 3.2) is also made out of a polyurethane tube (1.27 cm ID) filled by a packed array of copper rods that together act as a thermal reservoir. Filter papers on either end of the regenerator keep the rods in place. Both the chambers and the regenerator are mounted and secured to an aluminum frame. A summary of the relevant dimensions of the main components used in the setup is provided in Table 3.1.

K-type 30 gage thermocouples are inserted into the flexible chamber to measure the air temperature inside the chambers during operation. The time constant of the thermocouples was measured to be 3.6 s. The thermocouples and the electronic valves controlling the pneumatic actuators are connected to a data acquisition system

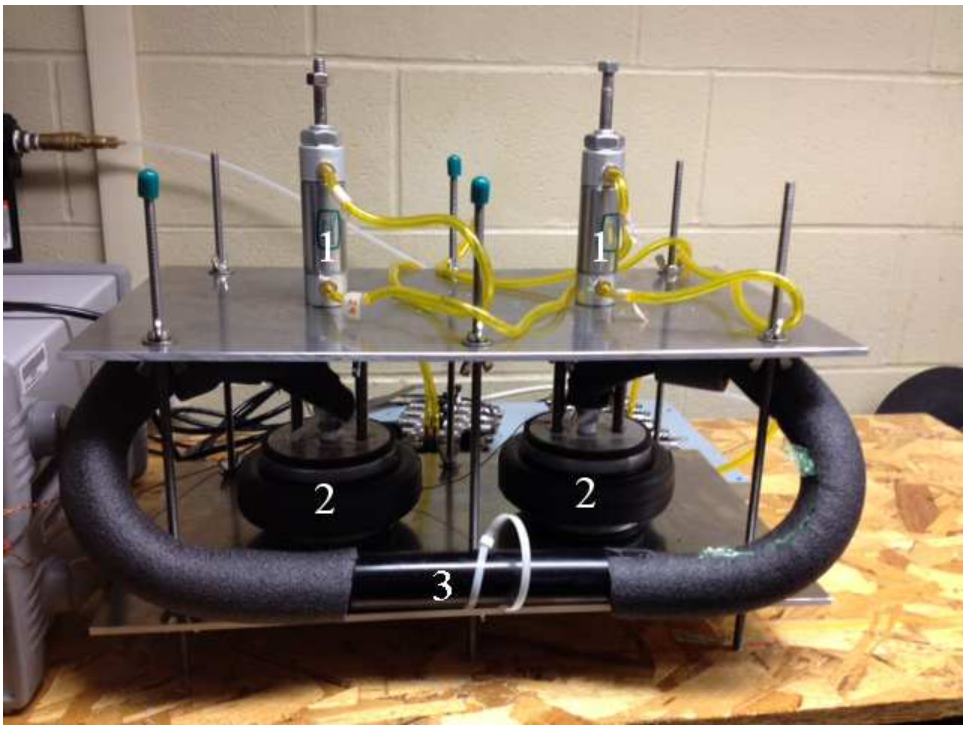

Figure 3.2. Photograph of Stirling refrigerator. (1), (2) and (3) indicate two pneumatic actuators, two flexible chambers, and regenerator, respectively. Distance between centerlines of the two chambers is 18.6 cm.

running a LabVIEW code. The computer outputted square wave signals to the valves to open and close them as desired; for periodic input the open and closed intervals were equal. The nature and period of these square waves could be programmed. The computer also acquired the signal from the thermocouples, transformed them into temperatures using a calibration provided by the manufacturer (40 μV/K), and stored the data. The temperature differences measured were considered small enough for the calibrations of the two thermocouples to be considered locally linear. The offset between the two thermocouples when they were at the same temperature was subtracted out to provide a correct measurement of the temperature difference.

TABLE 3.1

Component dimensions

Quantity	Value
Chamber volume	533 cm^3
Regenerator length	14 cm
Regenerator ID (without copper rods)	1.27 cm
Copper rods in regenerator	36
Copper rod diameter	2 mm
Actuator stroke	5.08 cm

3.2.2 TEST PROCEDURE

The performance of the experimental setup was based on measurements of the temperature difference between the two chambers of the Stirling refrigerator under different operating conditions. Each experimental data set was acquired by continuously operating the setup until steady-state conditions were reached. The chambers were allowed to rest between consecutive measurements to reach room temperature (which is the initial condition for the next test). For each run, the absolute value of the temperature difference between the two chambers, $\Delta T(t)$, was measured and recorded as a function of time t. The chamber that led in phase was always warmer than the other; with this in mind, only the absolute value of the temperature difference is needed.

In particular the effects of three parameters were investigated: the frequency of actuation f, the amplitude of the external air pressure oscillation P_H and P_L, and the phase angle between the motion of the chambers ϕ. Nominal operation was at $f = 1$ Hz, $\Delta P = P_H - P_L = 172.4$ kPa, and $\phi = 90°$. When one parameter was varied, the others were kept at the nominal values.

3.2.3 TESTING OF SET-UP

First, to check the uncertainty in the experimental measurements, five independent data sets were acquired for the nominal conditions. The results are shown in Fig. 3.3. The variation in the results could be due to errors in measurement or most likely due to changes in environmental conditions which were not controlled. The average steady-state temperature difference is 3.08 K with a standard deviation of 0.39 K (or 12.7 % of the steady-state temperature difference for the ensemble). This standard deviation, since it represents an uncertainty in the results of independent runs, is used for the error bars in later results. Each curve was fitted to an

exponential of the form

$$\Delta T(t) = \Delta T_f(1 - e^{t/\tau}), \tag{3.1}$$

going from $\Delta T = 0$ to $\Delta T = \Delta T_f$ as $t \to \infty$. The time constant τ of each run was determined; the average time constant for the ensemble was 10.47 mins. The temperature difference dynamics must be viewed in the context of the thermocouple time constant: the small-time temperature fluctuations are probably not correctly followed by the thermocouples, but the long-time overall trend is.

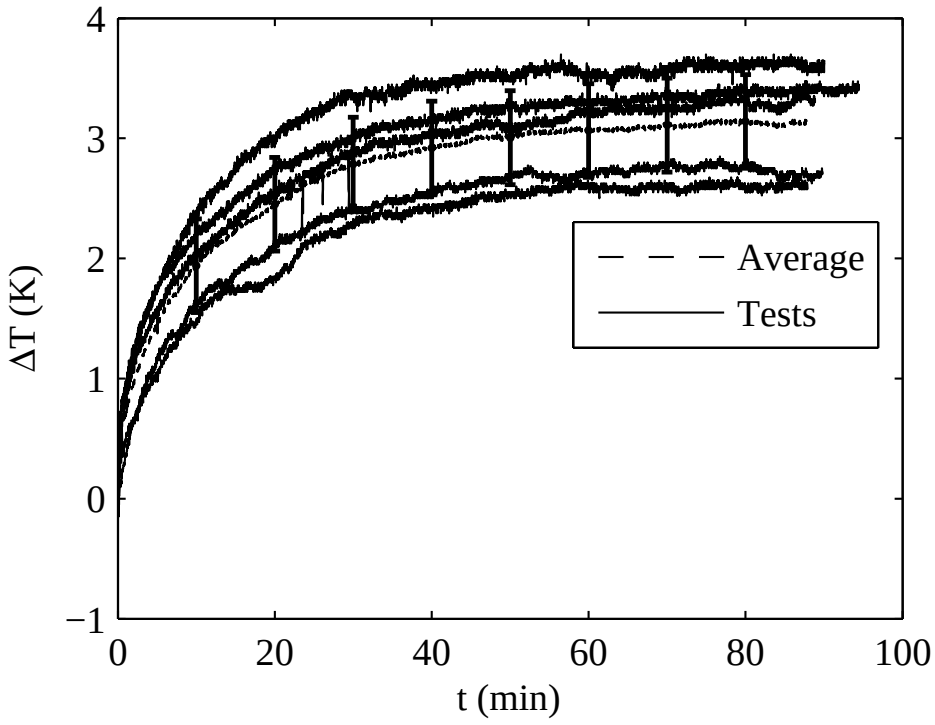

Figure 3.3. Instantaneous temperature difference between the flexible chambers for five independent tests. The average is also shown, as well as the standard deviation at different times.

CHAPTER 4

EXPERIMENTAL RESULTS

4.1 RESULTS

The setup was used to acquire multiple data sets under different operating conditions in order to analyze the effect of the functional parameters. The effect of these parameters is compared with respect to the nominal operating condition. Each run has an exponential-like $\Delta T(t)$ behavior as shown in Fig. 3.3. The steady-state value ΔT_f is of interest.

4.1.1 EFFECT OF FREQUENCY

During this test, the frequency of actuation f of the pressure input to the flexible chambers was varied in order to assess the effect on the steady-state temperature difference, ΔT_f. The frequency was changed in the 1 to 2 Hz range, considered to be relevant to human body-motion energy harvesting applications, was tested using increments of 0.25 Hz; all the other parameters were held constant at their nominal values. Fig. 4.1 shows the results of ΔT measurements for $f = 1$ Hz. At steady state, ΔT_f is about 3.6 K. Fig. 4.2 summarizes the value of ΔT_f for different f, and it is seen to go down with increasing f.

This result is significantly different from that in a motion-driven refrigerator. In the latter, the amplitude of the volume displaced every cycle is fixed, and with higher frequencies of operation, the same phenomenon takes place every period and the heat flow rate increases per unit time. Here, however, the flexible chamber has to respond

to the variation of the difference between the external and internal pressures. As the input frequency increases, the chamber cannot respond to the pressure difference quickly enough and the volume displaced per cycle goes down. Hence, the ΔT_f decreases with increasing f in Fig. 4.2.

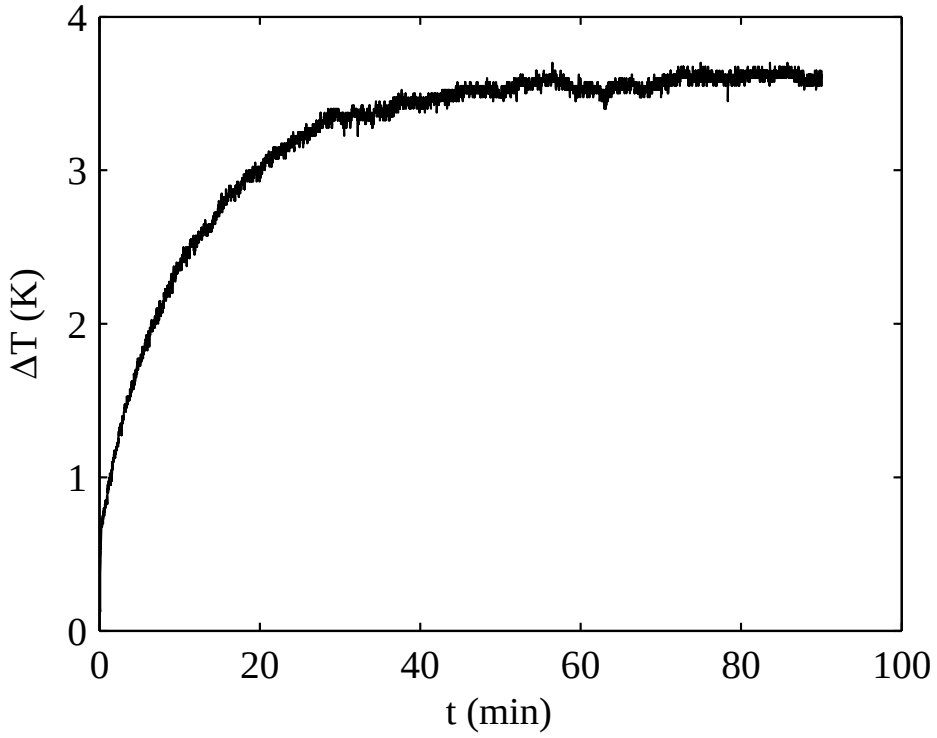

Figure 4.1. Chamber temperature difference for a frequency of 1 Hz.

4.1.2 EFFECT OF AIR PRESSURE AMPLITUDE

The second parameter to be investigated was the external pressures applied to the flexible chambers. The pressures can be varied in two different ways..

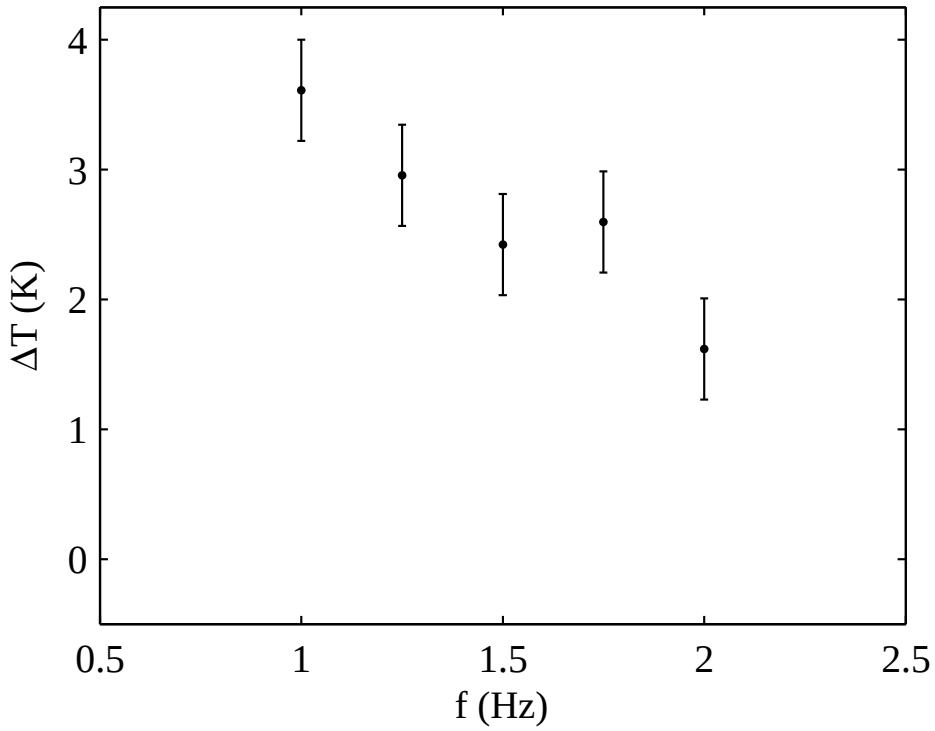

Figure 4.2. Temperature difference between chambers in steady state with varying frequencies.

In the first series of runs, the pressure difference between the actuators $\Delta P = P_H - P_L$ was kept constant. The low pressure was at $P_L = 172.4$, 137.9, 103.4 and 68.9 kPa (i.e. 25, 20, 15, and 10 psi), with $\Delta P = 172.4$ kPa. The ΔT_f resulting from these tests is shown in Fig. 4.3, where the low pressure value is used for the abscissa.

In a second series of runs, $P_H = 344.7$ kPa while ΔP was varied. Fig. 4.4 shows ΔT_f for this case as a function of ΔP. The decrease in ΔT_f is due to the decrease in the amplitude of motion of the chambers caused by the decrease in the low pressure. This reduces the expansion of the working fluid in the refrigerator.

Fig. 4.5 is a plot of $\Delta T_f(P_L, P_H)$ from the data points in Figs. 4.3 and 4.4. It is evident that P_L has a much stronger effect on ΔT_f than P_H. The expansion and compression in each chamber depends on the pressure difference between the external and the internal pressures. For each chamber, the latter is dependent not only on

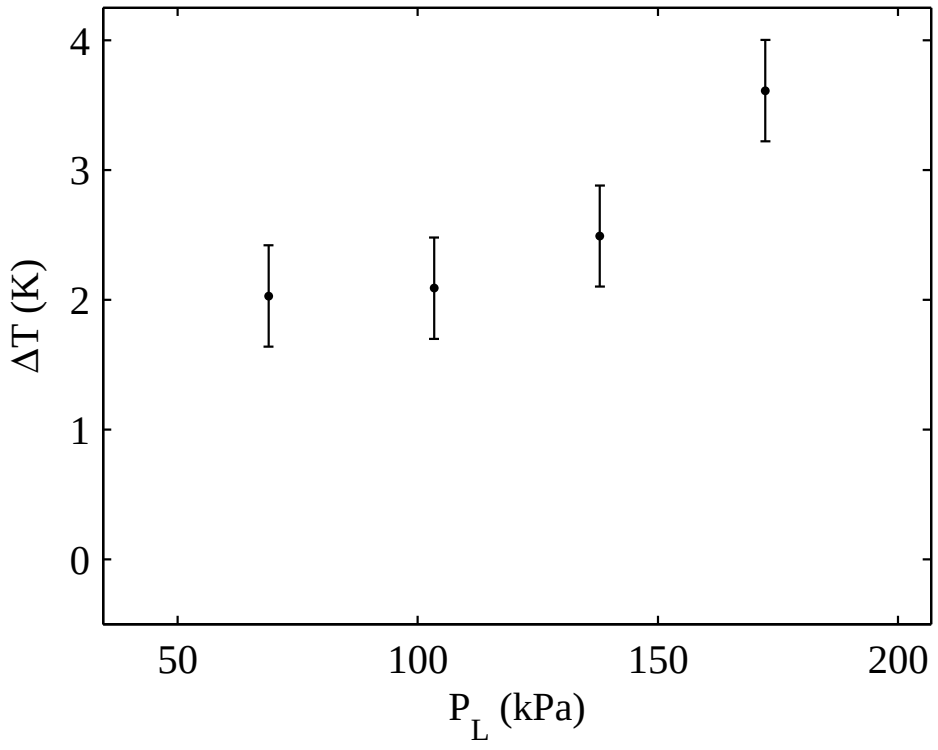

Figure 4.3. Temperature difference between chambers in steady state with varying the low pressure; pressure difference in each actuator constant at $\Delta P = 172.4$ kPa.

what is happening in that chamber, but also in the other. Furthermore, that time interval of compression is different from that of expansion, so that the rate of air flow through the regenerator is not the same for the two strokes. The data show that the amplitude of volume displacement depends more on P_L than P_H due to these factors.

4.1.3 EFFECT OF PHASE ANGLE

The phase angle ϕ between the input periodic square-wave signals sent to the actuators is crucial to the operation of this refrigerating device, and its variation is studied here. Unlike electric-motor actuated piston-cylinder arrangements where the phase angle is fixed by kinematics of the machine, the pressure-driven flexible chamber device permits, through software, a variety of operating phase angles. This

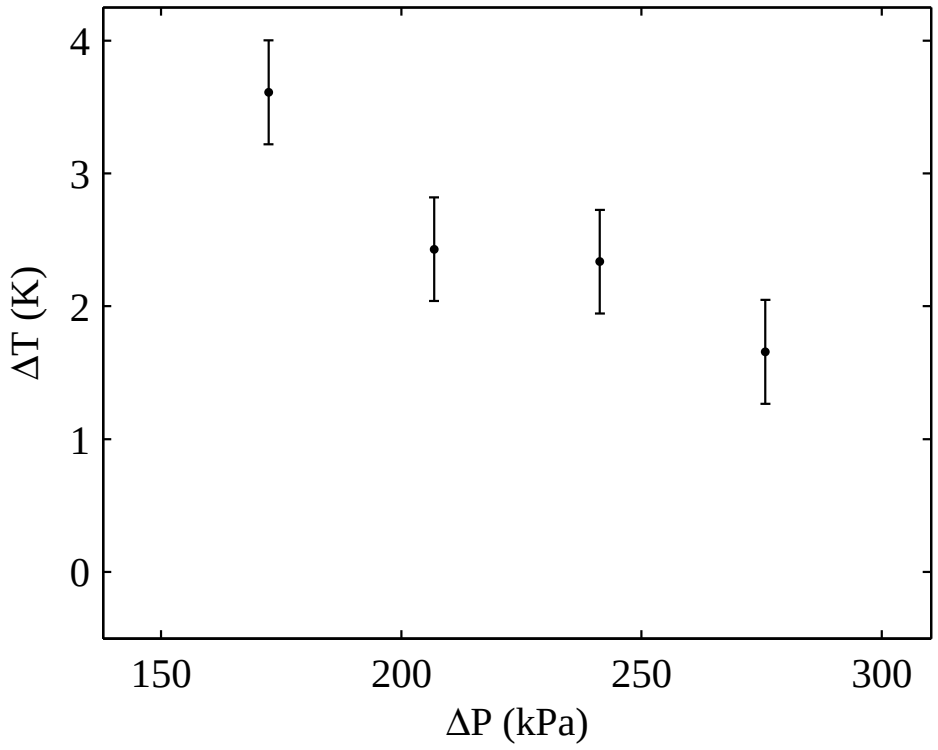

Figure 4.4. Temperature difference between chambers in steady state with varying pressure difference; high pressure constant at $P_H = 344.7$ kPa.

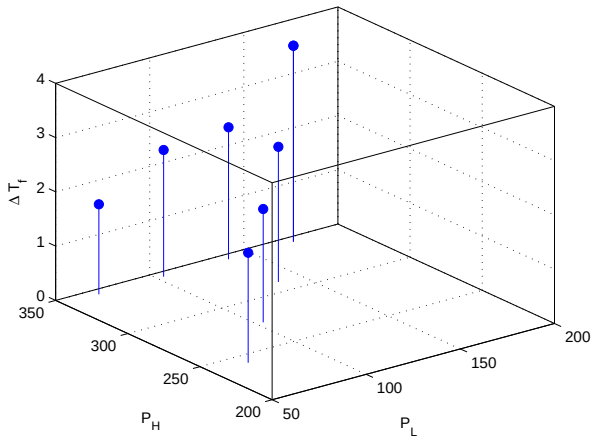

Figure 4.5. Effect of high and low pressures on steady-state temperature difference between chambers.

aspect is particularly important for application to a human-motion energy harvesting device where the input phase angle would be dictated by the specific ambulation conditions. Different input phase values in a $0° \leq \phi \leq 180°$ range were investigated using 15° increments while maintaining constant pressures and frequency at their nominal values.

Fig. 4.6 shows ΔT versus ϕ. The maximum ΔT_f is obtained around $\phi = 75°$. The minimum amount of cooling is obtained around $\phi = 0°$ and $\phi = 180°$; there is lack of air flow at $\phi = 0°$ phase because each chamber is compressed and expanded at the same time (i.e. perfectly in-phase), and there is lack of compression and expansion at $\phi = 180°$ due to the chambers having exact opposite motions (out-of-phase). If data were acquired for the range $\phi = 180°$ to $\phi = 360°$, the trend in Fig. 4.6 would be observed, the hot and cold chambers would be inverted.

4.1.4 EFFECT OF MODULATED INPUT

Of course, virtually no human motion is likely to provide a perfectly periodic input for any length of time. For this reason, the investigation of the performance of

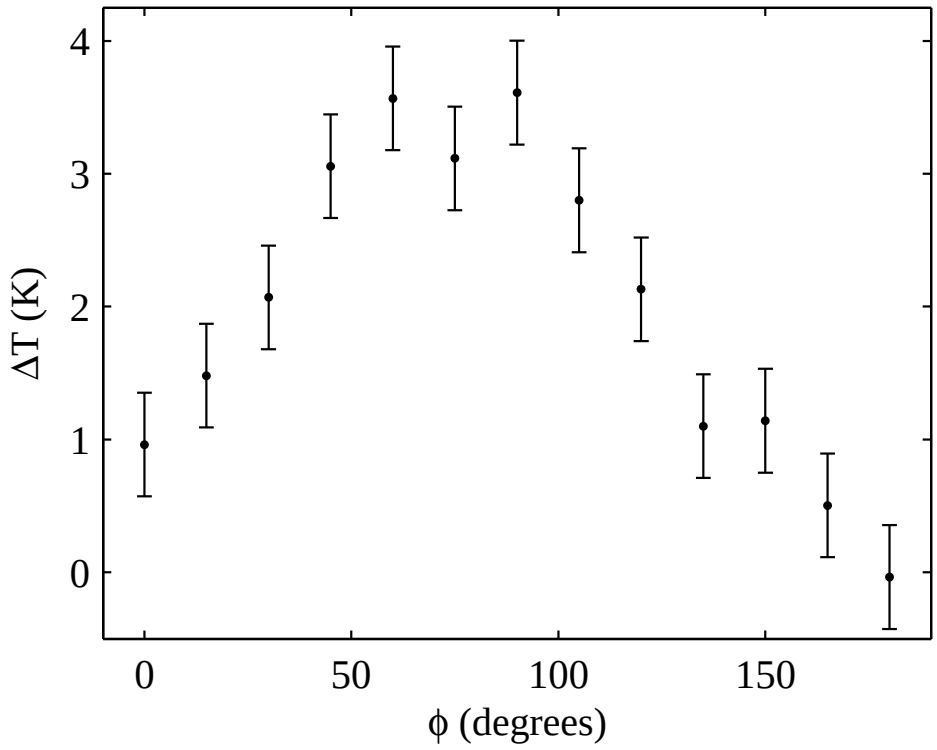

Figure 4.6. Temperature difference between chambers in steady state with varying phase angle.

the device under modulated inputs is of critical importance to assess the robustness of the refrigeration mechanism to variations in the driving conditions. Two tests, each altering the length of time that each chamber is compressed, were conducted. These pulse-shaped input signals to the refrigerator can be seen in Fig. 4.7 and Fig. 4.8. The lower value closes the valve and the upper value opens the valve. In Fig. 4.7, every *second* 'closed' portion of the square wave is half as long as the *previous* 'open' portion. In Fig. 4.8, every *second* 'closed' portion of the square wave is now twice as long as the *previous* 'closed' portion. The results can be seen in Fig. 4.9 and Fig. 4.10. Depending on the nature of the modulation, the steady state temperature can fluctuate almost 0.5 K. This demonstrates that the refrigerator still provides cooling or heating with modulated input, indicating a robust system. Fig. 4.11 and Fig. 4.12

show the fine-scale dynamics of the modulated inputs after 60 minutes of operation. While the complete results simply show the temperature fluctuation, the fine-scale dynamics reveal the structure present.

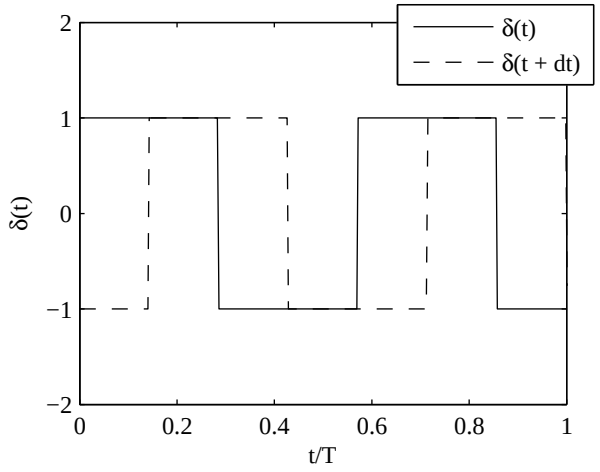

Figure 4.7. Modulated input signal to each pneumatic actuator for a period T.

Figs. 4.9 and 4.10 both show temperature differences comparable to those in Fig. 3.3. This demonstrates that the refrigerator provides cooling or heating even in the presence of modulated input, indicating a robust system. The fine-scale temperature differences shown in Figs. 4.7 and 4.8 show that there is some temperature fluctuation due to the modulation. The amplitude of the temperature fluctuation is somewhat under-measured, however, due to the 3.6 s time constant of the thermocouple.

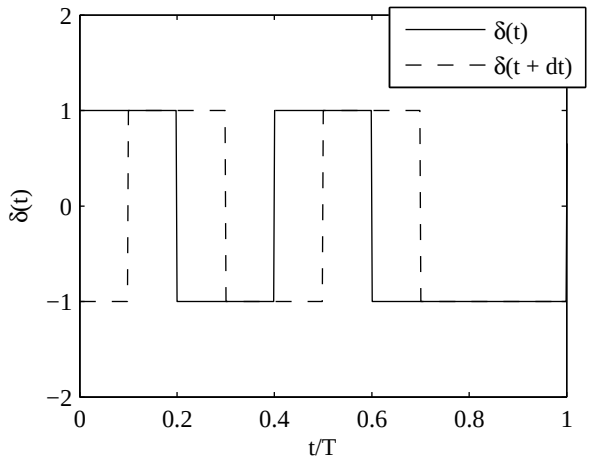

Figure 4.8. Modulated input signal to each pneumatic actuator for a period T.

4.2 DISCUSSION

An air-filled Stirling refrigerator with pressure-driven flexible chambers has been built and tested using inexpensive off-the-shelf items. The design of the apparatus and the experiments conducted reflect the focus on human-motion driven energy harvesting applications. The effect of varying system parameters on the temperature difference between the chambers has been experimentally evaluated. The results show that temperature differences in the 3-4 K range can be obtained, and that the operation is versatile and robust to changes in mechanical input. Details of the pressure-driven response are found to be different compared to motion-driven devices. High frequencies, for example, are not very useful because of a decrease in the volume of air exchanged between chambers.

Though there is a heat flow from one chamber to the other during operation, this cannot be calculated directly from a measurement of the temperature difference alone. In fact, ΔT is determined by this heat flow as well as the appropriate convective and conductive heat losses from the device to the environment. The heat flow heats and

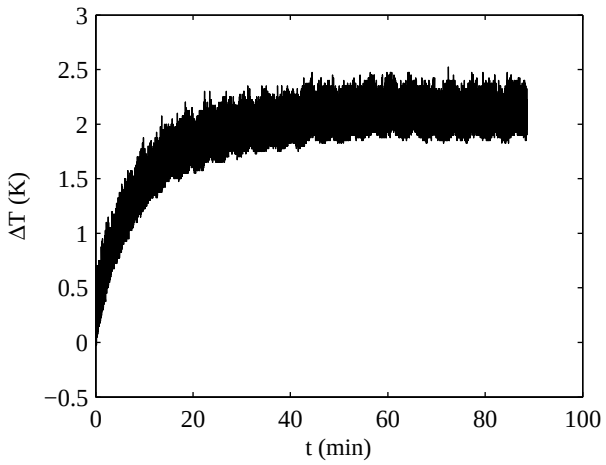

Figure 4.9. Temperature difference between chambers for the modulated input in Fig. 4.7.

cools not only the air, but also the mass of material around it. However, in an energy harvesting application, one may generally be interested in the temperature differences generated.

The time constant of the device is of the order of $\tau = Mc/UA$, where M, A and c are the mass, surface area and average specific heat per unit mass of the device, respectively, and U is the overall heat transfer coefficient between the air inside the chambers and the environment. If $M \sim L^3$ and $A \sim L^2$, where L is the size of the device, it appears that τ will be linear with L. Thus, a similar refrigerator that is ten times smaller will have a time constant around 1.05 min, which is very reasonable for a human-motion driven device. Further work needs to be done to determine the optimal operating parameters under actual working conditions. Reducing the mass of the device will also reduce τ, and changing the pressure-displacement characteristics of the flexible chamber will alter the volume flow rates of air exchange between chambers and hence the temperature differences achieved.

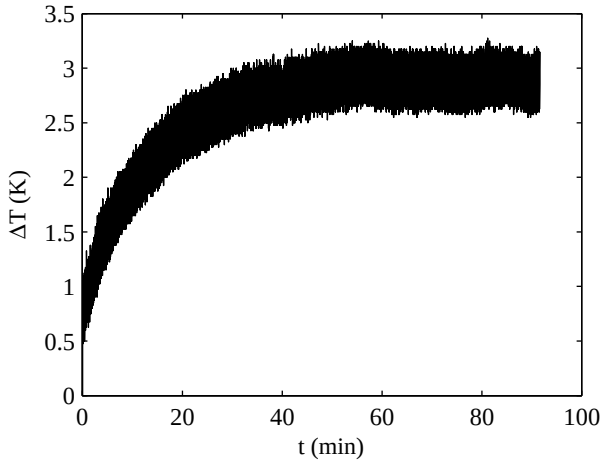

Figure 4.10. Temperature difference between chambers for the modulated input in Fig. 4.8.

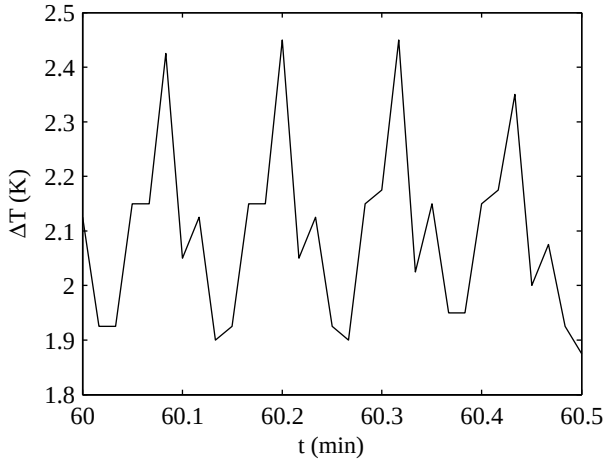

Figure 4.11. Temperature difference between chambers for a 30 s interval after 60 mins for the modulated input in Fig. 4.7.

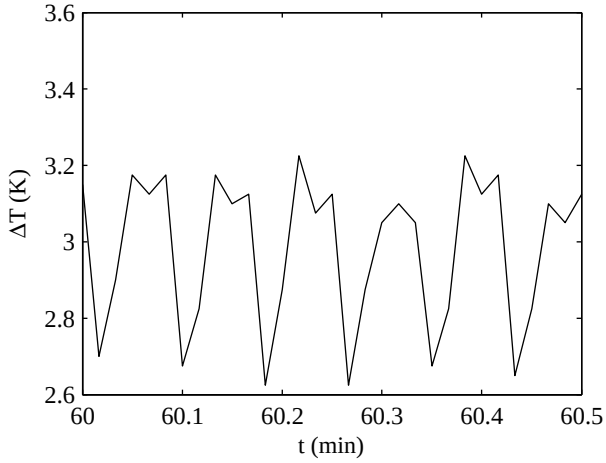

Figure 4.12. Temperature difference between chambers for a 30 s interval after 60 mins for the modulated input in Fig. 4.8.

CHAPTER 5

CONCLUSIONS AND RECOMMENDATIONS

5.1 CONCLUSIONS

5.1.1 MATHEMATICAL MODEL

The mathematical model developed here serves as a comprehensive representation of the operation of a Stirling refrigerator. By minimizing the assumptions and limitations of previous studies, this model can be used and manipulated for a variety of different initial conditions, sizes, and applications. The governing equations are derived for both chambers and the regenerator using the basic conservation and transport laws. The model allows for heat transfer in each section of the refrigerator at any time. The results show a clear temperature difference between the two chambers, a net cooling power of 1.9037 J per cycle, and a COP of 1.0706 for chamber 1. Mathematically, this indicates that a small Stirling refrigerator could be used as an energy harvesting device.

This section also derives the nondimensional forms of the governing equations in order to examine the effects of the physical parameters on refrigerator performance. The resulting nondimensional groups of parameters that control the system are identified. A sensitivity analysis is carried out in which several parameters were varied and plotted with the resulting nondimensional heat transfer. By holding all other parameters constant, the effects of these parameters on refrigerator performance were isolated and analyzed. This analysis can be used as a guide for refrigerator design for applications.

5.1.2 PHYSICAL MODEL

For the physical model, an air-filled alpha Stirling refrigerator with flexible chambers, keeping human-motion driven energy harvesting applications in mind, has been built and tested. The effect of varying system parameters on the temperature difference between the chambers has been experimentally evaluated. The results show that temperature differences in the 3–4 K range can be obtained, and that the operation is versatile and robust to changes in mechanical input. This work provides data previously unavailable for the viability of the Stirling refrigerator as an energy harvesting device powered by human-motion.

5.1.3 RECOMMENDATIONS

Both the mathematical model and physical model provide comprehensive data and analysis to support the claim that the Stirling refrigerator is capable of thermoacoustic energy harvesting for cooling applications. However, to further realize this, more work and research must be done.

The author recommends that a mathematical model of a flexible-chamber Stirling refrigerator be derived and tested. The mathematical model in this work considers only a rigid piston-cylinder arrangement. This flexible chamber mathematical model could then be more directly compared to the physical model of this work.

For the physical model, further work needs to be done to reduce the size of the device and determine its optimal operating parameters under actual working conditions. To accomplish this, the author recommends construction of a smaller Stirling refrigerator that could be successfully installed and tested directly into a shoe or other article of clothing. This would produce the data necessary to conclude if a Stirling refrigerator could provide adequate cooling or heating to the user.

Appendices

.1 Mathematical Model MATLAB Code

```
%% nondimensional.m
% This program runs a simulation of an alpha Stirling refrigerator. NOTE:
% The simulation takes a little bit due to the small spatial and time
% steps.
% 4/24/14
%% Program
% Chamber Dimensions
clear
clc
close all

diameter = 10;
D = 0.05;% Piston diameter m



A = pi*(D/2)^2; % Piston cross sectional area m^2

Dr = 0.005; % Regenerator tube diameter m
Ar = pi*(Dr/2)^2; % Regenerator tube cross sectional area m^2
Pr = Dr*pi; % Regenerator tube perimeter m
Lr = 0.1; % Regenerator tube length m

% Convection Coefficients for each chamber
h1 = 100; % W/(m^2 K) Convection Coefficient for Chamber 1
h2 = 100; % W/(m^2 K) Convection Coefficient for Chamber 2
h = 100; % W/(m^2 K) Convection Coefficient for regenerator

cv = 718; % J/(kg K) for air
R = 287; % J/(kg K) for air
cp = cv+R; %J/(kg K) for air
cpw = 466; %J/(kg K) for steel of regenerator walls
rho_steel = 7850; % kg/m^3 density of steel of regenerator walls
mw = 1; % kg, mass of the steel of regenerator walls

omega = 1.5; % rad/s Frequency of piston motion
phi = pi/2; % rad Phase shift in motion of Piston 2
alpha = 0; % rad Phase shift in motion of Piston 1

dt=1.e-4; % s timestep
t_fin=(4*pi)/omega; % s final time
nstep=t_fin/dt; % Number of time increments
```

```
xhat1 = 0.05; % m, amplitude of piston 1 motion
xhat2 = 0.05; % m, amplitude of piston 2 motion
x2_o = 0.1; % m, initial position of piston 2
x1_o = 0.1; % m, initial position of piston 1

t = linspace(0,t_fin,nstep); % Duration of vibration (s)
t_star = (t*omega)/(2*pi); % Nondimensional Time
dt_star = t_star(2) - t_star(1); % Nondimensional Time Step

% Chamber Wall Temperatures
Tw1 = 300; % K constant for this model
Tw2 = 300; % K constant for this model

% Initial Conditions
u(1) = 0; %m/s flow velocity
P1(1) = 101325; % N/m^2 Chamber 1 air pressure
P2(1) = 101325; % N/m^2 Chamber 2 air pressure
T1(1) = 300; % K Chamber 1 air temperature
T2(1) = 300; % K Chamber 2 air temperature
x1(1) = x1_o + xhat1*sin(alpha); % m Piston 1 position
x2(1) = x2_o + xhat2*sin(phi); % m Piston 2 position
m1(1) = (P1(1)*pi*x1(1)*(D/2)^2)/(R*T1(1)); % kg Chamber 1 air mass
m2(1) = (P2(1)*pi*x2(1)*(D/2)^2)/(R*T2(1)); % kg Chamber 2 air mass
rho1(1) = m1(1)/(A*x1(1)); % kg/m^3, Chamber 1 air density
rho2(1) = m2(1)/(A*x2(1)); % kg/m^3, Chamber 2 air density
mr(1) =(P1(1)*Ar*Lr)/(R*300); % kg, Regenerator air mass
rho = mr(1)/(Ar*Lr); %kg/m^3, density of air in regenerator
v1(1) = xhat1*omega*cos(alpha); % m/s Piston 1 velocity
v2(1) = xhat2*omega*cos(phi); % m/s Piston 2 velocity

Q1(1) = 0; % J, initial heat transfer in Chamber 1
Q2(1) = 0; % J, initial heat transfer in Chamber 2
W1(1) = 0; % J, initial work done in Chamber 1
W2(1) = 0; % J, initial work done in Chamber 2
V(1) = A*x1(1) + A*x2(1) + Ar*Lr; % m^3, refrigerator volume
V1(1) = A*x1(1); % m^3, Chamber 1 volume
V2(1) = A*x2(1); % m^3, Chamber 2 volume
mass(1) = m1(1) + m2(1) + rho*Ar*Lr; % kg, refrigerator air mass

% Values to nondimensionalize pressure, temperature
Tbar = Tw1; % K, initial air temperature
Pbar = P1(1); % N/m^2, initial air pressure
v = V1(1)/m1(1); % m^3, initial Chamber 1 volume
vmin = (((x1_o-xhat1)*A)/m1(1)); % m^3, minimum volume of Chamber 1
```

```
% K, air temperature if chambers were compressed adiabatically
delT = Tbar*(v^0.4 -vmin^0.4)*(1/(vmin^0.4));
% N/m^2, air pressure if chambers were compressed adiabatically
delP = Pbar*(v^1.4 -vmin^1.4)*(1/(vmin^1.4));


dx = 1.e-3; % m length step
x_fin = Lr; % m length of tube
dxstep = x_fin/dx; % Number of length steps

x(1:dxstep,1) = linspace(0,x_fin,dxstep); % m Position along tube from
x_star = x/Lr; % Nondimensional regenerator length
dx_star = x_star(2)-x_star(1); % Nondimensional spatial step
% Chamber 1 (0) to Chamber 2 (Lr)


Tw(1) = 300; % K Regenerator Wall initial temperature
for j = 1:dxstep
Tr(j,1) = 300; % K Regenerator Air initial temperature
Tr_star(j,1) = 0;
end
initial = 2; % The role of initial is to reset the condition for switching
% between the governing equations for the regenerator air temperature.
% Initial is only changed when the flow reverses directions. If you follow
% the logic of initial in the code, it basically ensures that every time
% the flow switches directions, the initial condition is at the time of the
% switch, and not time 0 or any other time.

% Nondimensional Groups (see text)
B1_1 = x1_o/xhat1;
B1_2 = x2_o/xhat2;
B2_1 = (2*h1*pi^2*D*xhat1)/(cv*mass(1)*omega);
B2_2 = (2*h2*pi^2*D*xhat2)/(cv*mass(1)*omega);
B3 = (2*pi*R*Tbar)/(cv*delT);
B4_1 = (delP*pi*D^2*xhat1)/(4*mass(1)*cv*delT);
B4_2 = (delP*pi*D^2*xhat2)/(4*mass(1)*cv*delT);
B5_1 = (Pbar*pi*D^2*xhat1)/(4*mass(1)*cv*delT);
B5_2 = (Pbar*pi*D^2*xhat2)/(4*mass(1)*cv*delT);
B6 = Pbar/delP;
B7_1 = (4*mass(1)*R*Tbar)/(delP*xhat1*pi*D^2);
B7_2 = (4*mass(1)*R*Tbar)/(delP*xhat2*pi*D^2);
B8_1 = (4*mass(1)*R*delT)/(delP*xhat1*pi*D^2);
B8_2 = (4*mass(1)*R*delT)/(delP*xhat2*pi*D^2);
B9 = (rho*Dr*cp*omega)/(8*pi*h);
```

```
B10 = (mass(1)*omega*cp)/(h*pi*Dr*Lr);
B11 = (2*h*pi^2*Dr*Lr)/(mw*cpw*omega);
B12 = sqrt((rho*pi^2*Dr^5*delP)/(32*Lr*0.1*mass(1)^2*omega^2));

Bnew_1 = (2*pi*delP)/(rho*cv*delT);
Bnew_2 = (Pbar*2*pi)/(rho*cv*delT);

%% Numerical Integration
% This loop evaluates each variable at time t(i). Individual terms are
% explained in the loop

% Nondimensional Parameters (see text)
x1_star(1) = B1_1;
x2_star(1) = B1_2 + sin(phi);
v1_star(1) = 2*pi;
v2_star(1) = 2*pi*cos(phi);
T1_star(1) = (T1(1) - Tbar)/delT;
T2_star(1) = (T2(1) - Tbar)/delT;
M1_star(1) = m1(1)/mass(1);
M2_star(1) = m2(1)/mass(1);
P1_star(1) = (P1(1)-Pbar)/delP;
P2_star(1) = (P2(1)-Pbar)/delP;
Tw1_star = 0;
Tw2_star = 0;
Tw_star(1) = (Tw(1)-Tbar)/delT;
mdot_star(1) = 0;
V1_star(1) = x1_star(1)*A;
for i = 2:nstep
    x1_star(i) = B1_1 + sin(2*pi*t_star(i)); % Piston 1 position
    x2_star(i) = B1_2 + sin(2*pi*t_star(i) + phi); % Piston 2 position
    v1_star(i) = 2*pi*cos(2*pi*t_star(i)); % Piston 1 velocity
    v2_star(i) = 2*pi*cos(2*pi*t_star(i) + phi); % Piston 2 velocity

    V1_star(i) = x1_star(i)*A; % Chamber 1 volume

if mdot_star(i-1) > 0 %Chamber temperature equations if flow is postive

T1_star(i) = T1_star(i-1) + dt_star*(1/M1_star(i-1))*(B2_1*x1_star(i-1)*...
        (Tw1_star - T1_star(i-1)) - mdot_star(i-1)*...
        (Bnew_1*P1_star(i-1) + Bnew_2) - (B4_1*P1_star(i-1) + B5_1)*...
        v1_star(i-1));
 % T1_star is the temperature of the air in Chamber 1 (Euler's method)
T2_star(i) = T2_star(i-1) + dt_star*(1/M2_star(i-1))*(B2_2*x2_star(i-1)*...
    (Tw2_star - T2_star(i-1)) + (2*pi*mdot_star(i-1)*...
```

```
    (Tr_star(dxstep,i-1) - T2_star(i-1)) + mdot_star(i-1)*...
    (Bnew_1*P2_star(i-1) + Bnew_2)) - (B4_2*P2_star(i-1) + B5_2)*...
    v2_star(i-1));
   % T2_star is the temperature of the air in Chamber 2 (Euler's method)
elseif mdot_star(i-1) < 0%Chamber temperature equations if flow is negative
     % T1_star is the temperature of the air in Chamber 1 (Euler's method)
T1_star(i) = T1_star(i-1) + dt_star*(1/M1_star(i-1))*(B2_1*x1_star(i-1)*...
    (Tw1_star - T1_star(i-1)) - (2*pi*mdot_star(i-1)*...
    (Tr_star(1,i-1) - T1_star(i-1)) + mdot_star(i-1)*...
    (Bnew_1*P1_star(i-1) + Bnew_2)) - (B4_1*P1_star(i-1) + B5_1)*...
    v1_star(i-1));
    % T2_star is the temperature of the air in Chamber 2 (Euler's method)
T2_star(i) = T2_star(i-1) + dt_star*(1/M2_star(i-1))*(B2_2*x2_star(i-1)*...
    (Tw2_star - T2_star(i-1)) + mdot_star(i-1)*...
    (Bnew_1*P2_star(i-1) + Bnew_2) - (B4_2*P2_star(i-1) + B5_2)...
    *v2_star(i-1));
else % Governing chamber temperature if there is no flow
T1_star(i) = T1_star(i-1) + dt_star*(1/M1_star(i-1))*(B2_1*x1_star(i-1)*...
    (Tw1_star - T1_star(i-1)) - (B4_1*P1_star(i-1) + B5_1)*v1_star(i-1));
     % T1_star is the temperature of the air in Chamber 1 (Euler's method)
T2_star(i) = T2_star(i-1) + dt_star*(1/M2_star(i-1))*(B2_2*x2_star(i-1)*...
    (Tw2_star - T2_star(i-1)) - (B4_2*P2_star(i-1) + B5_2)*v2_star(i-1));
     % T2_star is the temperature of the air in Chamber 2 (Euler's method)
end


     % Mass in Chamber 1 (Euler's method)
    M1_star(i) = M1_star(i-1) + dt_star*(-2*pi*mdot_star(i-1));
    % Mass in Chamber 2 (Euler's method)
    M2_star(i) = M2_star(i-1) + dt_star*(2*pi*mdot_star(i-1));



    P1_star(i) = ((B7_1*M1_star(i) + B8_1*M1_star(i)*...
        T1_star(i))/(x1_star(i))) - B6; % Pressure in Chamber 1
    P2_star(i) = ((B7_2*M2_star(i) + B8_2*M2_star(i)*...
        T2_star(i))/(x2_star(i))) - B6; % Pressure in Chamber 2



    if P1_star(i)>=P2_star(i)
    mdot_star(i) = B12*sqrt((P1_star(i)-P2_star(i))); % Mass flow rate
    else
     mdot_star(i) = -B12*sqrt(-(P1_star(i)-P2_star(i))); % Mass flow rate
```

```
end



% This loop is only engaged when the flow switches directions (place a
% debugger inside this loop to verify). Then, initial is set to the
% current i so that initial conditions and times are referred to this
% point. Also, step and reverse_step measure if a particular point in
% the tube is still subject to the transient delay. So, when the flow
% switches directions, the transient delay comes back, and these
% numbers again measure that delay from the time of the flow switching
% directions.
if (mdot_star(i)*mdot_star(i-1)) <= 0 && i>3
    initial = i;
    step(i) = 0;
    reverse_step(i) = 0;
end

% This loop, the subsequent summation, and finally the use of Euler's
% method obtains the temperature of the regenerator wall at time t(i).
% The loop gets the heat transfer contribution from sections of the
% regenerator tube of length dx. Summing these individual contributions
% effectively executes a Euler's method along the regenerator tube.
% Then, an Euler's method with respect to time is used to get the wall
% temperature at time t(i).
for j = 1:dxstep
    int(j,i) = dx_star*(Tw_star(i-1) - Tr_star(j,i-1));
end
sum_length(i) = sum(int(:,i));
Tw_star(i) = Tw_star(i-1) + dt_star*(-B11*sum_length(i));

% This loop obtains the regenerator air temperature when the flow is
% zero. Obviously, the only way the temperaure of the fluid can change
% when there is no flow is by heat transfer from the walls of the
% regenerator.
if mdot_star(i) == 0
   for j = 1:dxstep
   Tr_star(j,i) = Tr_star(j,i-1) + dt_star*(1/(B9))*...
       (Tw_star(i-1) - Tr_star(j,i-1));
   end
end
```

```
   % This loop obtains the regenerator air temperature when the flow is
   % greater than 0. The role of step is to discern whether the
   % temperature at the particular x location is affected by the flow yet.
   % If the transient delay is still occurring, then the first equation is
   % used. If the transient delay is over, then the second equation is
   % used.
   if mdot_star(i)>0
       for j = 1:dxstep
           step(i) = dt*(mdot_star(i)*mass(1)*omega*(1/(rho*Ar)));
           if x(j,1)>sum(step(initial:i))
               Tr_star(j,i) = (Tr_star(j,i-1))+ dt_star*...
                   (1/(B9))*(Tw_star(i-1) - Tr_star(j,i-1));
           else
               Tr_star(j,i) = (T1_star(i)-Tw_star(i))*...
                   exp(-(x(j,1)/Lr)/(B10*mdot_star(i))) + Tw_star(i);
           end
       end
   end

      % This loop obtains the regenerator air temperature when the flow is
   % less than 0. The role of reverse_step is to discern whether the
   % temperature at the particular x location is affected by the flow yet.
   % If the transient delay is still occurring, then the first equation is
   % used. If the transient delay is over, then the second equation is
   % used.
   if mdot_star(i)<0
       for j = 1:dxstep
           reverse_step(i) = dt*(mdot_star(i)*mass(1)*omega*(1/(rho*Ar)));
           if x(j,1)>-sum(reverse_step(initial:i))
               Tr_star(dxstep+1-j,i) = (Tr_star(dxstep+1-j,i-1))+...
                   dt_star*(1/(B9))*(Tw_star(i-1) - Tr_star(j,i-1));
           else
               Tr_star(dxstep+1-j,i) = (T2_star(i)-Tw_star(i))*...
                   exp((x(j,1)/Lr)/(B10*mdot_star(i))) + Tw_star(i);
          end
       end
   end

   % Nondimensional Heat and Work. NOTE: Dividing by 4.188 divides by the
   % period of this particular cycle! If you change the frequency, you'll
   % have to change this value
Q1_star(i) = (h1/100)*(D/0.05)*(xhat1/0.05)*x1_star(i)*(2*pi/(omega))*...
    (Tw1_star - T1_star(i))*(dt_star/4.188);
Q2_star(i) = (h2/100)*(D/0.05)* (xhat2/0.05)*x2_star(i)*(2*pi/(omega))*...
```

```
     (Tw2_star - T2_star(i))*(dt_star/4.188);
 W1_star(i) = (-v1_star(i)/(2*pi))*(P1_star(i) + Pbar/delP)*dt_star;
 W2_star(i) = (-v2_star(i)/(2*pi))*(P2_star(i) + Pbar/delP)*dt_star;

end

% NOTE: This sums the heat from the beginning to the end of cycle 2, which
% goes from t_star(4188:4188*2). If you change the period/frequency, you
% must change this so it captures the entire period of a cycle!
% Nondimensional heat transfer in chamber 1 over the second cycle
DIMENSIONLESS_HEAT1 = sum(Q1_star(4188:4188*2));
% Nondimensional heat transfer in chamber 2 over the second cycle
DIMENSIONLESS_HEAT2 = sum(Q2_star(4188:4188*2));

% Plots, plot what you'd like! These are the plots in the text, but you can
% alter them as you like.
plot(V1_star(4188:4188*2 ),P1_star(4188:4188*2 ),'LineWidth',2)
figure(2)
axis([1 2 1 3])
plot(t_star(4188:4188*2 ), T1_star(4188:4188*2 ), 'LineWidth',2)
hold on
plot(t_star(4188:4188*2 ),P1_star(4188:4188*2 ),'--', 'LineWidth', 2)
hold on
plot(t_star(4188:4188*2 ), M1_star(4188:4188*2 ), ':','LineWidth', 2)
hold on
plot(t_star(4188:4188*2 ), x1_star(4188:4188*2 ),'-.', 'LineWidth',2)
hold on
axis([1 2 1 3])
figure(3)
plot(t_star(4188:4188*2 ), T2_star(4188:4188*2 ), 'LineWidth',2)
hold on
plot(t_star(4188:4188*2 ),P2_star(4188:4188*2 ),'--', 'LineWidth', 2)
hold on
plot(t_star(4188:4188*2 ), M2_star(4188:4188*2 ), ':','LineWidth', 2)
hold on
plot(t_star(4188:4188*2 ), x2_star(4188:4188*2 ),'-.', 'LineWidth',2)
hold on
axis([1 2 1 3])
figure(4)
plot(t_star(4188:4188*2 ),mdot_star(4188:4188*2 ),'LineWidth',2)
figure(5)
plot(t_star(4188:4188*2 ),Q1_star(4188:4188*2 ),'LineWidth',2)
hold on
plot(t_star(4188:4188*2 ),Q2_star(4188:4188*2),'--','LineWidth',2)
```

1

BIBLIOGRAPHY

1. P. McFarlane, F. Semperlotti, and M. Sen. Mathematical model of an air-filled alpha stirling refrigerator. *Journal of Applied Physics*, 114, 2013.

2. P. McFarlane, J. Suire, M. Sen, and F. Semperlotti. Experiments with a pressure-driven stirling refrigerator with flexible chambers. *Journal of Applied Physics*, 2014, under review.

3. W.B. Gosney. *Principles of Refrigeration*. Cambridge University Press, Cambridge, U.K., 1982.

4. B. Kongtragool and S. Wongwises. Thermodynamic analysis of a Stirling engine including dead volume of hot space, cold space, and regenerator. *Renewable Energy*, 31:345–359, 2006.

5. J. Liang. Thermodynamic cycles in oscillating flow regenerators. *Journal of Applied Physics*, 82(9):4159–4165, 1997.

6. Gianfranco Angelino and Costante Invernizzi. Potential performance of real gas Stirling cycle heat pumps. *International Journal of Refrigeration*, 19(6):390–399, 1996.

7. Feng Wu, Lingen Chen, Chin Wu, and Fengrui Sun. Optimum performance of irreversible engine with imperfect regeneration. *Energy Conversion and Management*, 39(8):727–732, 1998.

8. S.C. Kaushik and S. Kumar. Finite time thermodynamic analysis of endoreversible Stirling heat engine with regenerative losses. *Energy*, 25:989–1003, 2000.

9. V.S. Chakravarthy, R.K. Shah, and G. Venkatarathnam. A review of refrigeration methods in the temperature range 4-300k. *Journal of Thermal Science and Engineering Applications*, 3, 2011.

10. D.G. Thombare and S.K. Verma. Technological development in the Stirling cycle engines. *Renewable and Sustainable Energy Reviews*, 12:1–38, 2006.

11. A.T.A.M. de Waele. Basic operation of cryocoolers and related thermal machines. *Journal of Low Temperature Physics*, 164(5-6):179–236, 2011.

12. Y. Tekin and O.E. Ataer. Performance of V-type Stirling-cycle refrigerator for different working fluids. *International Journal of Refrigeration*, 33:12–18, 2010.

13. O.E. Ataer and H. Karabulut. Thermodynamic analysis of the V-type Stirling cycle refrigerator. *International Journal of Refrigeration*, 28:183–189, 2005.

14. J. Chen and Z. Yan. The general performance characteristics of a Stirling refrigerator with regenerative losses. *Journal of Physics D: Applied Physics*, 29:987–990, 1996.

15. L.B. Erbay and H. Yavuz. The maximum cooling density of a realistic Stirling refrigerator. *Journal of Physics D: Applied Physics*, 31:291–293, 1997.

16. D. Omari. *Mathematical Modeling of Thermocompressive and Thermoacoustic Machines*. PhD thesis, University of Notre Dame, Department of Chemical Engineering, Notre Dame, IN 46556, August 1996.

17. K.D. Timmerhaus and T.M. Flynn. *Cryogenic Process Engineering*. Plenum Press, New York, NY, 1989.

18. G.W. Swift. *Thermoacoustics*. Acoustical Society of America, Melville, NY, 2002.

19. M.R. Osorio, A.P. Morales, J.G. Rodrigo, H. Suderow, and S. Vieira. Demonstration experiments for solid-state physics using a table-top mechanical stirling refrigerator. *European Journal of Physics*, 33(4):757–770, 2012.

20. T. Ki and S. Jeong. Step-by-step design methodology for efficient stirling-type pulse tube refrigerator. *International Journal of Refrigeration*, 35(4):1166–1175, 2011.

21. D.S. Antao and B. Farouk. Experimental and numerical investigations of an orifice type cryogenic pulse tube refrigerator. *Applied Thermal Engineering*, 50(1):112–123, 2013.

22. E.C. Luo, W. Dai, Y. Zhang, and H. Ling. Experimental investigation of a thermoacoustic-stirling refrigerator driven by a thermoacoustic-stirling heat engine. *Ultrasonics*, 44:E1531–E1533, 2006.

23. L. Sun, Y.Y. Zhao, L.S. Li, and P.C. Shu. Performance of a prototype stirling domestic refrigerator. *Applied Thermal Engineering*, 29(2-3):210–215, 2009.

24. X.N. He, M.Q. Gong, H. Zhang, W. Dai, J. Shen, and J.F. Wu. Design and performance of a room-temperature hybrid magnetic refrigerator combined with stirling gas refrigeration effect. *International Journal of Refrigeration*, 36(5):1465–1471, 2013.

25. K. Tang, J. Yu, T. Jin, and Z.H. Gan. Influence of compression-expansion effect on oscillating-flow heat transfer in a finned heat exchanger. *Journal of Zhejiang University-Science A*, 14(6):427–434, 2013.

This document was prepared & typeset with pdfLaTeX*, and formatted with* NDdiss2$_\varepsilon$ *classfile (v3.2013[2013/04/16]) provided by Sameer Vijay and updated by Megan Patnott.*